








Cite this: *J. Mater. Chem. C*, 2018, **6**, 12121

## Electrically conductive polymer composites for smart flexible strain sensors: a critical review

Hu Liu, \*<sup>abc</sup> Qianming Li,<sup>a</sup> Shuaidi Zhang,<sup>a</sup> Rui Yin,<sup>a</sup> Xianhu Liu, <sup>a</sup> Yuxin He,<sup>d</sup> Kun Dai, <sup>a</sup> Chongxin Shan,<sup>b</sup> Jiang Guo,<sup>e</sup> Chuntai Liu,<sup>\*a</sup> Changyu Shen,<sup>a</sup> Xiaojing Wang,<sup>cf</sup> Ning Wang,<sup>g</sup> Zicheng Wang,<sup>ch</sup> Renbo Wei \*<sup>h</sup> and Zhanhu Guo \*<sup>c</sup>

The rapid development of wearable smart devices has contributed to the enormous demands for smart flexible strain sensors. However, to date, the poor stretchability and sensitivity of conventional metals or inorganic semiconductor-based strain sensors have restricted their application in this field to some extent, and hence many efforts have been devoted to find suitable candidates to overcome these limitations. Recently, novel resistive-type electrically conductive polymer composites (ECPCs)-based strain sensors have attracted attention based on their merits of light weight, flexibility, stretchability, and easy processing, thus showing great potential applications in the fields of human movement detection, artificial muscles, human-machine interfaces, soft robotic skin, etc. For ECPCs-based strain sensors, the conductive filler type and the phase morphology design have important influences on the sensing property. Meanwhile, to achieve a successful application toward wearable devices, several imperative features, including a self-healing capability, superhydrophobicity, and good light transmission, need to be considered. The aim of the present review is to critically review the progress of ECPCs-based strain sensors and to foresee their future development.

Received 14th August 2018,  
Accepted 12th October 2018

DOI: 10.1039/c8tc04079f

rs.c.li/materials-c

<sup>a</sup> Key Laboratory of Materials Processing and Mold (Zhengzhou University), Ministry of Education, National Engineering Research Center for Advanced Polymer Processing Technology, Zhengzhou University, Zhengzhou, 450002, China. E-mail: liuhu@zzu.edu.cn, ctliu@zzu.edu.cn

<sup>b</sup> School of Physics and Engineering, Zhengzhou University, Zhengzhou, Henan 450052, China

<sup>c</sup> Integrated Composites Laboratory (ICL), Department of Chemical & Biomolecular Engineering, University of Tennessee, Knoxville, TN 37996, USA. E-mail: zgao10@utk.edu

<sup>d</sup> College of Chemical Engineering and Pharmaceutics, Henan University of Science and Technology, Luoyang, Henan 471023, China

<sup>e</sup> School of Materials Science & Engineering, Shaanxi University of Science & Technology, Xi'an 710021, China

<sup>f</sup> School of Material Science and Engineering, Jiangsu University of Science and Technology, Zhenjiang, Jiangsu, 212003, China

<sup>g</sup> State Key Laboratory of Marine Resource Utilization in South China Sea, Hainan University, Haikou 570228, China

<sup>h</sup> Research Branch of Advanced Functional Materials, School of Materials and Energy, University of Electronic Science and Technology of China, Chengdu, 611731, China. E-mail: weirb10@uestc.edu.cn



Hu Liu

Dr Hu Liu is an associate professor at the National Engineering Research Center for Advanced Polymer Processing Technology of Zhengzhou University. He obtained his PhD from Zhengzhou University (2017), and then worked as a joint PhD student with Prof. Zhanhu Guo at the University of Tennessee, Knoxville, USA, sponsored by the China Scholarship Council (2015–2016). His current research interest focuses on multifunctional polymer-based nanocomposites, especially conductive polymer composite-based sensors, electromagnetic shielding materials, and thermal insulating aerogel.



Qianming Li

Mr Qianming Li, currently a degree candidate in National Engineering Research Center for Advanced Polymer Processing Technology at Zhengzhou University (Supervisor: Prof. Changyu Shen), obtained his bachelor degree in College of Chemical Engineering and Pharmaceutics at Henan University of Science and Technology (2018). His research interest focuses on multifunctional polymer based nanocomposites for strain sensors and superhydrophobicity applications.

# 1 Introduction

With the accelerating development of wearable smart devices, the demand for high-performance smart flexible strain sensors is growing. They have shown great prospects in various applications, including human movement detection,<sup>1–12</sup> body health monitoring,<sup>13</sup> artificial muscles, soft robotic skin,<sup>14</sup> human-machine interfaces,<sup>15</sup> and structure health monitoring.<sup>16</sup> However, traditional strain sensors are generally composed of metals or inorganic semiconductor, which cannot satisfy the imperative requirement for high-strain sensing capabilities due to their limited detection range (5%).<sup>17–22</sup> Besides, the complex preparation process involved and high fabrication cost also restrict their application and development. Thus, novel smart flexible strain sensors are in urgent demand, and relevant research efforts have also emerged as highly promising topics.



**Shuaidi Zhang**

*Mr Shuaidi Zhang, currently a Master degree candidate in National Engineering Research Center for Advanced Polymer Processing Technology at Zhengzhou University (Supervisor: Prof. Chuntai Liu), obtained his bachelor degree (2017) from School of Materials Science and Engineering at Luoyang Institute of Science and Technology. His research interests focus on multifunctional polymer nanocomposites for wearable electronic sensors.*



**Chuntai Liu**

*Dr Chuntai Liu is currently a professor at the National Engineering Research Center for Advanced Polymer Processing Technology (NERC) of Zhengzhou University. He obtained his PhD from Zhengzhou University (2003), and then worked as a visiting scholar at Ohio State University, USA (2006–2007). He serves as the deputy director of NERC of Zhengzhou University. His research focuses on multifunctional polymer composites, including their processing and microstructure properties.*



**Zhanhu Guo**

*Dr Zhanhu Guo, an Associate Professor in the Department of Chemical and Biomolecular Engineering, University of Tennessee, Knoxville, USA, obtained a PhD degree in Chemical Engineering from Louisiana State University (2005) and received three-year (2005–2008) postdoctoral training from the Mechanical and Aerospace Engineering Department at the University of California Los Angeles. Dr Guo chaired the Composite Division of the American Institute of Chemical Engineers (AIChE, 2010–2011) and directs the Integrated Composites Laboratory. His current research focuses on multifunctional nanocomposites for education, transportation, safety, information, catalysis, energy harvesting and storage, electronics and environmental remediation applications.*

Recently, functional polymer-based composites have exhibited great potential in the fields of electrical/thermal conductive materials,<sup>23–27</sup> flame retardants,<sup>28–31</sup> dielectrics,<sup>32–36</sup> electromagnetic interference (EMI) shielding,<sup>37,38</sup> self-healing,<sup>39</sup> bio-immobilization,<sup>40</sup> energy,<sup>41–46</sup> environment remediation,<sup>44,47–51</sup> anticorrosion coating,<sup>52</sup> and sensors.<sup>53–62</sup> All these are ascribed to the perfect combination of the characteristics of the polymer matrix (*e.g.*, low density, easy processing, and good flexibility) and functional fillers (*e.g.*, high thermal/electrical conductivity, magnetism, and excellent mechanical property). Among these, electrically conductive polymer composites (ECPCs) have turned out to be intriguing candidates for smart flexible strain sensors based on the variation of electrical resistance upon different external strain,<sup>63–72</sup> including stretching, compression, bending, and twisting. The good flexibility and stretchability of the polymer matrix enable the ECPC-based strain sensors to be knitted,<sup>73–78</sup> skin-attachable,<sup>13</sup> and wearable,<sup>79–81</sup> showing its superiority over conventional ones. Hence, tremendous efforts have been devoted to the investigation of new generation ECPC-based smart flexible strain sensors.

Normally, ECPCs are obtained through the combination of conductive fillers with an insulating polymeric matrix using suitable processing technology (*e.g.*, solution mixing, melt compounding, *in situ* polymerization, spray-coating, spin-coating, and dip-coating). With increasing filler loading, continuous conductive networks are built based on the junction of adjacent conductive fillers, and the insulator/conductor transition is generally observed at a critical content, which is termed the electrical percolation threshold ( $P_c$ ).<sup>82</sup> Since one of the first studies about the transition published in 1966,<sup>83</sup> it has become a research hotspot in the field. ECPCs with a lower  $P_c$  could effectively reduce the production cost and maintain the processability and mechanical properties of ECPCs on the basis of their good electrical property.<sup>84,85</sup> Therefore, a number of methods have

been applied to achieve this goal, such as the addition of large aspect ratio nanofillers or synergistic bifillers,<sup>86–92</sup> and the construction of special phase morphology (e.g., segregated structure,<sup>93–99</sup> double percolation structure,<sup>100–102</sup> and porous structure<sup>65,69,103</sup>). In addition, being smart flexible strain sensors, the choices of the polymer matrix and conductive fillers are the crucial factors for its sensing performance. Generally, elastomers with large elongation and good flexibility, including thermoplastic polyurethane (TPU),<sup>59,65,67,68,71,104–108</sup> rubber,<sup>4,22,109–115</sup> ecoflex,<sup>6,9,116–118</sup> and poly(dimethylsiloxane) (PDMS),<sup>2,8,14,17–20,119–123</sup> are the most widely selected polymers in previous publications, showing great potential applications for the fabrication of strain sensors with a wide strain range. Meanwhile, electrically conductive fillers, such as carbonaceous fillers (e.g., carbon nanotubes (CNTs), carbon black (CB), grapheme, and carbon fiber (CF)),<sup>27,124–128</sup> intrinsically conductive polymers (e.g., PEDOT:PSS, PPy and PANI),<sup>129–132</sup> and nanometals (e.g., silver nanowire/nanoparticles, gold nanosheets, and Cu nanowire),<sup>3,13,16,21,70,133–140</sup> are often used to endow the composites with excellent electrically conductive property. Then, a suitable processing technique was adopted to blend them together to construct an effective conductive network. The reported various ECPC-based strain sensors and their performances are summarized in Table 1.

Viewed from the present research situation of ECPC-based strain sensors, a wide sensing range, high sensitivity, high resolution, rapid response, good durability, and excellent environmental stability are the imperative characters that need to be satisfied. It is known that its working principle is mainly based on the variation of electrical resistance caused by the rearrangement of the conductive network when ECPCs are exposed to an external strain/stress. Generally, the type and geometric morphology of the conductive filler affect the conductive network morphology, generating significant influences on the sensing performance of a sensor.<sup>141–146</sup> Besides, construction of a special conductive network is also an effective method to tune ECPCs' sensing behavior.<sup>59,147–151</sup> Hence, to achieve these imperative characteristics as stated above, the choice of conductive filler type and its morphology and the design of a highly

active conductive network using special processing technology are the two crucial factors to be considered. ECPCs with a different conductive network morphology and their performance are also summarized in Table 2.

Until now, the published review papers about ECPCs have mainly focused on the regulation of ECPCs' electrical properties. However, recent progress in ECPC-based smart flexible strain sensors has yet to be systematically addressed in any review. For instance, Xie and coworkers systematically reviewed the recent extensive progress in ECPCs with controllable electrical properties by designing a segregated structure and double percolation structure.<sup>64</sup> Deng and coworkers entirely summarized the processing approaches used to tune the morphology of the conductive network, and their influence on ECPCs' electrical properties. Meanwhile, the multifunctionalities (e.g., strain and damage sensing, stretchable conductor, temperature sensing, vapor and liquid sensing, shape memory, and thermoelectric materials) of ECPCs have also been comprehensively reviewed.<sup>152</sup> Pang and coworkers systematically discussed the influence factors of the percolation behaviors of CPCs with a segregated structure, and its potential applications in the fields of sensing/thermoelectricity/EMI shielding were also reviewed.<sup>153</sup> Motivated by the discussion above, the latest development of ECPC-based smart flexible strain sensors are critically reviewed in this paper. The second part presents the basic mechanism of ECPC-based strain sensors. In the third part, the strain-sensing behaviors of ECPCs filled with different types of conductive fillers are comprehensively introduced with detailed examples. In the fourth part, ECPCs with improved sensing properties by designing a special conductive network (e.g., segregated structure, porous structure, micro-crack structure, and wrinkled structure) are discussed. In the fifth part, several imperative features (e.g., self-healing capability, superhydrophobicity, and good light transmission) for advanced ECPC-based strain sensors are introduced. In the final part, the above parts are concluded and the outlook for ECPC-based smart flexible strain sensor are presented.

Table 1 The reported various ECPC-based strain sensors and their performance

Polymer matrix	Conductive filler	Processing technique	Properties	Ref.
PU	CB	Layer by layer	GF = 39; tiny strain limit = 0.1%; wearable	1
TPU	CNT	Diffusion process	Sensing range: 400%	105
TPU	Graphene	Coagulation/hot pressing	GF = 0.78–17.7; sensing range: 30%; wearable	68
PU	PPy	Situ polymerization	Sensing range: 100%; wearable	213
PU	PEDOT:PSS	Fiber wet-spinning	Sensing range: 160%; knittable	104
PDMS	CNT film	Cast coating	Sensing range: 280%; response time: 14 ms; GF = 0.06–0.82	8
PDMS	CNT/PU-PEDOT:PSS	Spin coating	GF = 62; transparent; sensing range: 100%; wearable	15
PDMS	RGO	Cast coating	GF = 630; sensing range: 50%	18
PDMS	Graphene fabrics	Spin coating	GF = 10 <sup>3</sup> (2–6%), 10 <sup>6</sup> (>7%) and 35 (0.2%)	2
Rubber	Graphene	Solution soaking	GF = 35; sensing range: 6%	4
Ecoflex	Gold	Contact transfer	GF = 70.3 (<50%) and 37.8 (50–70%)	3
SBS	CNT-Ag NP	Absorption- <i>in situ</i> reduction	GF = 26 500; sensing range: 540%	109
SBS	AgNW-Ag NP	Wet spinning	Sensing range: 100%; wearable	10
POE	AgNW	Diffusion process	GF = 13920; tiny strain limit = 0.065%; knittable	75
PP	CB CNT	Melting blend and hot compression	Sensing range: 3%	163
PC	CNT	Melt spinning	GF = 2.5–16	173

Table 2 ECPCs with different conductive network morphology and their performance

Conductive network morphology	Composites	Properties	Ref.
Micro-crack structure	PUA/Pt	GF = 2000 under 0–2% strain; detection ability: 10 nm	149
	PDMS/gold	Controllable crack; sensing range: 100%	214
	TPU/AgNW/RGO	Tiny strain limit = 0.3%; GF = 4000	106
Porous structure	PU sponge/CB	Tiny strain limit = 0.2%; response time = 20 ms	193
	TPU/graphene foam	Compression strain = 90%; GF = 2.45 (< 60%) and 24 (60–90%)	65
	PI/RGO	Compression strain = 50%; pressure sensitivity = 0.18 kPa <sup>-1</sup> (0–1.5 kPa) and 0.023 kPa <sup>-1</sup> (3.5–6.5 kPa)	215
Segregated structure	NR/CNT	GF = 43.5; sensing range: 100%	110
	PDMS/CNT	GF = 142 at 30% compression strain	187
Wrinkled structure	Ecoflex/Pt	GF = 42; sensing range: 185%	13
	Ecoflex/CNT	GF = 0.65 (0–400%) and 48 (400–700%)	6

## 2 Fundamentals of ECPC-based strain sensors

### 2.1 Conductive mechanism of ECPCs

Due to the differences in polymers' physicochemical properties (*e.g.*, melting index, crystallinity, and molecular polarity) and conductive fillers' structure and morphology, the dispersion state of the conductive filler in the polymer matrix is unpredictable during the preparation process of ECPCs. Thus, there is still no unified conclusion of the conductive mechanism.

Generally, the conductive mechanism of ECPCs is closely related to the conductive filler loading and can be classified into two main types, one including a tunneling effect and the other Ohmic conductance (Fig. 1). A tunneling effect mainly exists in ECPCs with a lower filler loading, where most fillers are covered by a layer of polymer during the mixing procedure, forming a barrier higher than the free electron energy. According to the theory of classical mechanics, it is impossible for a free electron to hop the barrier when its energy is lower than the barrier height, impeding the effective electronic conduction. However, quantum mechanics proves that the microscopic particles with a lower energy than the barrier height still have some probability to hop the barrier, which is usually called the tunneling effect. For ECPCs, Balberg proposed the tunneling conduction model, expressed as eqn (1).<sup>154</sup>

$$\sigma_{\text{tun}} \propto \exp(-r/d) \quad (1)$$

where  $\sigma$  represents the tunneling conductivity,  $r$  represents the tunneling distance (the shortest distance between the center of the adjacent conductive filler), and  $d$  represents the tunneling decay parameter. It is obviously seen that  $\sigma$  is inversely proportional to  $r$ , so  $r$  is an important parameter to control the charge transfer between adjacent conductive fillers.<sup>155</sup> Generally,  $r$  decreases with

the increase in filler loading, causing a higher  $\sigma$ . When the filler loading is increased to the percolation threshold, the conductive networks distributed in the polymer matrix are constructed, providing relatively low-resistance electrical paths for the movement of free electrons, so the Ohmic conductance turns to be the main conductive mechanism in this circumstance gradually.

From a macro perspective, the change from the tunneling effect to Ohmic conductance with the increase in filler content is associated with the abrupt transition of ECPCs' conductivity, which is generally defined as the percolation theory. According to Flory's gelation theory, Kirkpatrick and Appel proposed the classical statistical percolation model, expressed as eqn (2), which was used to describe the relationship between the filler loading above  $P_c$  and the ECPCs' conductivity.

$$\sigma = \sigma_0(p - p_c)^t \quad (2)$$

where  $p$  represents the volume fraction of the conductive filler,  $\sigma$  and  $\sigma_0$  represent the conductivity of the ECPCs and conductive filler, respectively, and  $t$  is a scaling factor used to predict the dimensionality of the conductive network constructed in the ECPCs. Generally, two-dimensional (2D) and three-dimensional (3D) conductive networks were considered to be achieved when  $t$  is within the range of 1.1–1.3 and 1.6–2.0, respectively. Of course, higher or lower  $t$  values were also observed in some reports due to the complex distribution of the conductive filler, including ECPCs with a segregated structure<sup>93,156,157</sup> and porous structure.<sup>65,103</sup>

### 2.2 Response mechanism of ECPC-based strain sensors

ECPC-based strain sensors are a kind of resistive-type sensor, and their response mechanisms are mainly based on the variation of conductive networks upon external strain/stress, transferring the stimuli into a resistance signal. ECPCs with a filler loading above  $P_c$  are usually chosen to ensure a stable sensing behavior. Based on the conductive mechanism discussed above, different sensing mechanisms are generally proposed according to the applied strain amplitude: (1) under a small strain amplitude, the connections between neighboring fillers are not easy to be destructed, and the variation of the tunneling distance contributes to the resistance change, causing a small sensing signal; (2) with the strain amplitude

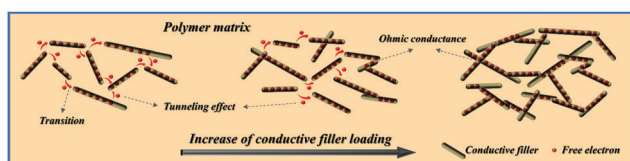


Fig. 1 Schematic illustration of the conductive mechanism of ECPCs.

increasing, the tunneling distance of some tunneling paths turns out to be larger than the cut-off distance. Meanwhile, some direct connections between the conductive filler are separated, leading to the destruction of the whole conductive network. All these undoubtedly induce a larger change in resistance than that under the small strain amplitude, thus showing a stronger sensing signal.<sup>158,159</sup>

Conversely, when the external strain was removed, most conductive paths will return to their initial state completely due to the good elasticity of the polymer matrix. However, there are still some conductive paths that are irreversible due to the hysteresis effect of the molecular chain of the polymer and the complete destruction of the unstable conductive path. All these tend to lead to residual resistance (higher resistance than the initial value) of ECPCs, causing bad recoverability when used as a strain sensor. In this case, cyclic tension or compression, choosing a proper polymer matrix, and designing a special conductive network are often adopted to stabilize the conductive network, endowing ECPCs with stable sensing behavior.

In addition, the gauge factor (GF), defined as the relative change in the electrical resistance per unit strain, is usually used to evaluate the strain sensitivity of resistive-type strain sensors. Generally, GF can be expressed as eqn (3):

$$GF = ((R - R_0)/R_0)/\varepsilon \quad (3)$$

where  $R_0$  is the initial resistance of CPCs and  $R$  is the resistance of ECPCs at the strain of  $\varepsilon$ .

### 3 Sensing performance of ECPCs with different conductive fillers

In this part, ECPCs filled with carbonaceous filler/metallic nanowires/hybrid fillers are systematically reviewed, and the influences of the filler type and geometric morphology on the reconfiguration mode of the conductive network and the strain sensing behavior upon external strain are analyzed and concluded, with an aim to provide a theoretical basis for the choice of conductive fillers.

#### 3.1 Carbonaceous fillers

According to a literature survey, carbonaceous fillers are the most widely employed for the fabrication of high-performance polymer-based composites with enhanced mechanical strength, abrasion resistance, stiffness, and thermal and electrical properties. As for ECPCs filled with different dimensional carbonaceous fillers (e.g., 0D CB, 1D CNT, and 2D graphene), their strain sensing behaviors have been widely investigated and compared, showing great potential application for the fabrication of a CPC-based strain sensor with the expected properties.

**0D CB.** As a cheap and commercially available carbon nanomaterial with good electrical conductivity, many efforts have been made to explore its application in strain sensors.<sup>120,143,160–166</sup> It can be seen from the SEM of CB (Fig. 2a) that the CB particles exist as aggregates with lots of branches, which is beneficial for the construction of effective conductive networks.<sup>163</sup> Meanwhile, the aggregation state also inevitably leads to a higher percolation threshold. As a strain sensor, the conductive network is easy to

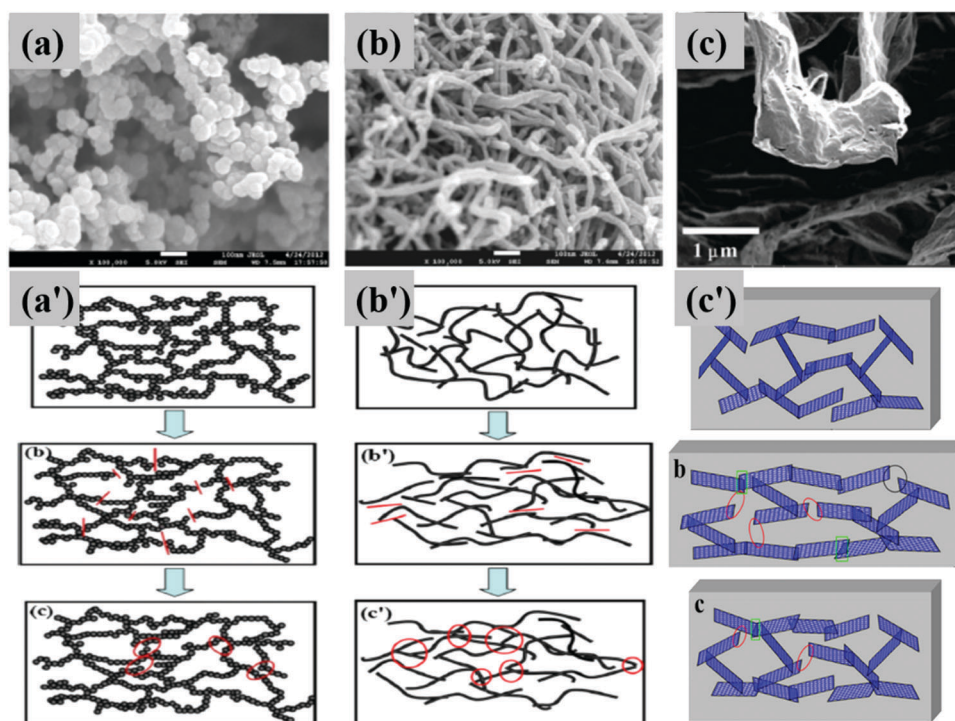


Fig. 2 SEM image of (a) CB, (b) CNT and (c) graphene; schematic illustration of the change in (a') CB, (b') CNT and (c') graphene conductive network in a single cycle (adapted with permission from ref. 68 and 163 Copyright 2013, Elsevier. Copyright 2016, Royal Society of Chemistry).

destruct because of the weak interaction between CB particles; however, some destructed conductive paths cannot revert back to their initial state after one loading cycle due to the hysteresis effect of the polymer matrix (Fig. 2a'). Hence, CB-based strain sensors usually exhibit an increasing trend in the initial several cycles due to the cumulative effect. According to the aggregation state of CB, it is generally divided into low structure CB, medium CB, and high structure CB. Numerous studies have been conducted to investigate their influence on the strain-sensing behavior.<sup>160,167–169</sup> For example, Yazdani and coworkers investigated the strain-sensing behavior of polyvinylchloride-based composites filled with medium structure CB and high structure CB, respectively.<sup>160</sup> The results indicated that the conductive networks consisted of higher-structure CB were not easy to destruct upon external tension and a greater degree of recoverability was achieved compared with ECPCs with a medium CB conductive network. Meanwhile, in the study of electrical CB filled nature rubber composites, Jha *et al.* also observed the fact that CPCs with a higher CB structure were beneficial for improvement of the recoverability of ECPCs.<sup>169</sup>

**1D CNT.** Based on the extraordinary electrical conductivity, one-dimensional (1D) CNTs are useful in electronic devices and sensor applications. According to the calculation of the particle number and simulation of their distribution of composites with the same filler volume fraction, ECPCs filled with CNT usually possess a very low percolation threshold due to its nano-sized diameter and large aspect ratio. In addition to the size effect, its special entangled structure (Fig. 2b) arising from the van der Waals force between individual CNTs usually endows ECPCs with a distinct strain-sensing behavior.<sup>163</sup> Recently, lots of related research works have been conducted to exploit its application potentiality.<sup>75,90,170–173</sup> For example, elastomeric TPU/CNT nanocomposites were fabricated through a solution mixture technique, and a low percolation threshold of about 0.35 wt% was achieved.<sup>170</sup> During the initial several cyclic loadings at 5% strain amplitude, due to the rearrangement of the entangled conductive networks and hysteresis effect of the polymer, some new conductive networks were constructed and a decreasing trend of ultimate resistance was observed (Fig. 2b'). After stabilization of the conductive network through cyclic loading, a monotonic strain sensing behavior with excellent recoverability and reproducibility was observed. However, the special entangled structure of CNTs also bring a nonmonotonic strain sensing style during a larger strain cycle, arising from competition between the destruction and construction of the conductive network, which is also frequently observed for other CNT-filled ECPCs.

**2D graphene.** Recently, the 2D graphene (Fig. 2c)<sup>68</sup> composed of a single layer of SP<sup>2</sup> hybridized carbon atoms has turned out to be the most important carbon nanomaterial and hence enormous efforts have been devoted to expand its applications in advanced polymer-based nanocomposites.<sup>174</sup> Besides, graphene possesses high carrier mobility, large specific surface area, and high-quality crystal lattice, all these make it an ideal carbon series conductive filler. Recently, ECPCs with an ultralow percolation threshold were successfully obtained for graphene/TPU (0.05 vol%),<sup>68</sup> graphene/polyurethane acrylate

(0.07 vol%),<sup>175</sup> and graphene/polystyrene (0.1 vol%)<sup>166</sup> nanocomposites due to their extraordinary electronic transport property, large specific surface area, and the aspect ratio of graphene. In addition, our group was the first to study graphene's application in the field of ECPC-based strain sensors. Graphene/TPU composites were fabricated using the co-coagulation plus compression molding technique, and a nearly 2D conductive network was constructed through the contact of a single graphene nanosheet.<sup>68</sup> Then, the influences of graphene loading, strain amplitude, and strain rate on the cyclic strain sensing performances were systematically investigated. Similar to CB-based ECPCs, irreversible resistance was also observed due to the hysteresis effect of the TPU molecular chain (Fig. 2c'). Hence, the ECPCs exhibited a growing trend in the first several cycles, but this tended to be balanced through stabilization of the graphene conductive network, showing good recoverability and reproducibility. In addition, it can be concluded that a lower graphene loading, larger strain amplitude, and higher strain rate are beneficial for the increase in GF, and a wide range of GF from 0.78 to 17.7 was obtained.

### 3.2 Metallic nanowires

Compared with carbon-based conductive fillers, 1D metallic nanowires, including silver nanowires, copper nanowires, and gold nanowires, have also exhibited great potential to serve as conductive filler for the fabrication of electronic device due to their outstanding electrical conductivity. Among all the metallic nanowires, silver nanowires possess the highest electrical conductivity ( $\sim 6.3 \times 10^7 \text{ S cm}^{-1}$ ),<sup>176</sup> thermal conductivity, and chemical stability. Besides, they also exhibit good oxidation resistance and corrosion resistance.<sup>134</sup> All these make silver-nanowires-filled ECPC-based strain sensors a research hotspot. For example, Lu *et al.* successfully prepared a conductive TPU electrospun membrane through vacuum filtration of a AgNW solution, and liquid PDMS was then spin-coated on its surface to form a flexible sandwich structure strain sensor (Fig. 3a).<sup>177</sup> As a result, it exhibited superb repeatability upon various strain amplitudes, and there was almost no obvious sensing drift during cyclic loading (Fig. 3b). In addition, the oxidation of silver nanowires in the air is a key factor influencing the durability of the sensing performance. In this study, due to the protection of the sandwich structure, there was almost no variation of conductivity when the sensor was exposed to the air for 30 days (Fig. 3c). Finally, its good flexibility makes it easy to attach on body parts to detect human motions, while its accurate and stable response proves its suitability to serve as a motion sensor (Fig. 3d).

### 3.3 Hybrid fillers

The synergistic effects in ECPCs filled with hybrid fillers have been proved as an effective method to enhance the dispersity of the nanofiller, leading to a lower percolation threshold. In addition, its superiority on tuning the sensing performance of sensors has also attracted much attention.<sup>10,21,59,75,129,134,178–184</sup> For example, Liu *et al.* studied the synergistic effect between 1D CNTs and 2D graphene and its influences on the strain-sensing

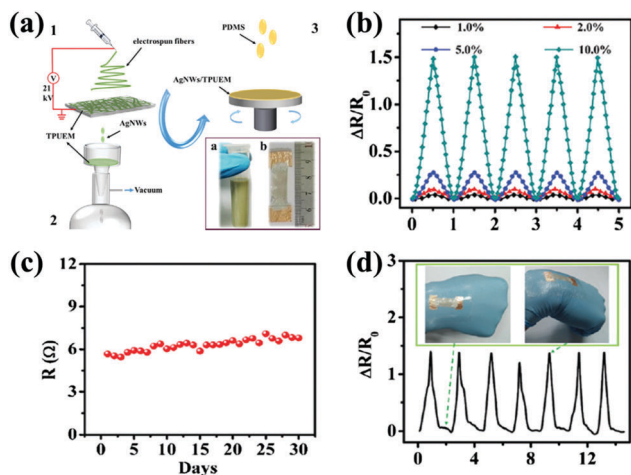


Fig. 3 (a) Schematic illustration for the fabrication of AgNW/TPU/PDMS strain sensor; (b) response of the sensor to cyclic stretching; (c) resistance versus time of the sensor in the air for 30 days; (d) responses of the strain sensor to cyclic wrist bending motion (adapted with permission from ref. 177 Copyright 2017, Royal Society of Chemistry).

behavior of TPU/CNT/graphene nanocomposites.<sup>59</sup> From the results, it can be seen that when a proper mass ratio is fixed, graphene could effectively separate the entangled CNT apart from each other and CNTs act as bridges to connect single graphene nanosheets (Fig. 4A(a)). All these are beneficial for reduction of the percolation threshold and construction of a sensitive conductive network. At a small strain of 5% (Fig. 4A(b)), compared with the dual-peak strain-sensing type of TPU/CNT nanocomposites, a

stable single-peak response mode was observed for TPU/CNT/graphene nanocomposites, showing a tunable sensing behavior with the assistance of the synergistic effect. However, TPU/CNT/graphene nanocomposites also exhibited an unstable dual-peak strain-sensing-type performance at a larger strain (15% and 30%), which may be due to the destruction of the stable synergistic conductive network (Fig. 4A(c)). In order to solve this problem, the authors successfully used the prestraining technique to regulate the conductive network. The study provided an effective way to achieve ECPCs with tunable strain-sensing behavior. In addition, Lee *et al.* fabricated a highly stretchable AgNW/SBS fiber using the wet spinning method, and then Ag nanoparticles were embedded into the fiber surface through repeat dipping in Ag precursor solution and *via* a reduction process.<sup>10</sup> For the synergistic conductive network, AgNWs act as a conducting bridge to link the separated Ag nanoparticles under large strain amplitude, ensuring effective electrical conductivity to enable it to serve as a strain sensor (Fig. 4B(a)). For the strain-sensing behavior at different strains (as high as 100%), it displayed a proportional response to the applied strain and good recoverability after the release of strain (Fig. 4B(b)). Moreover, the conductive fiber possesses great potential to be knitted into a wearable strain sensor to perceive human motions.

With the exception of the two different conductive fillers discussed above, the addition of a nonconductive nanofiller is also often applied. For instance, in order to solve the poor dispersion of AgNWs in a polymer matrix arising from the strong depletion-induced interaction between AgNWs, lots of hybrid systems have been widely investigated. For example,

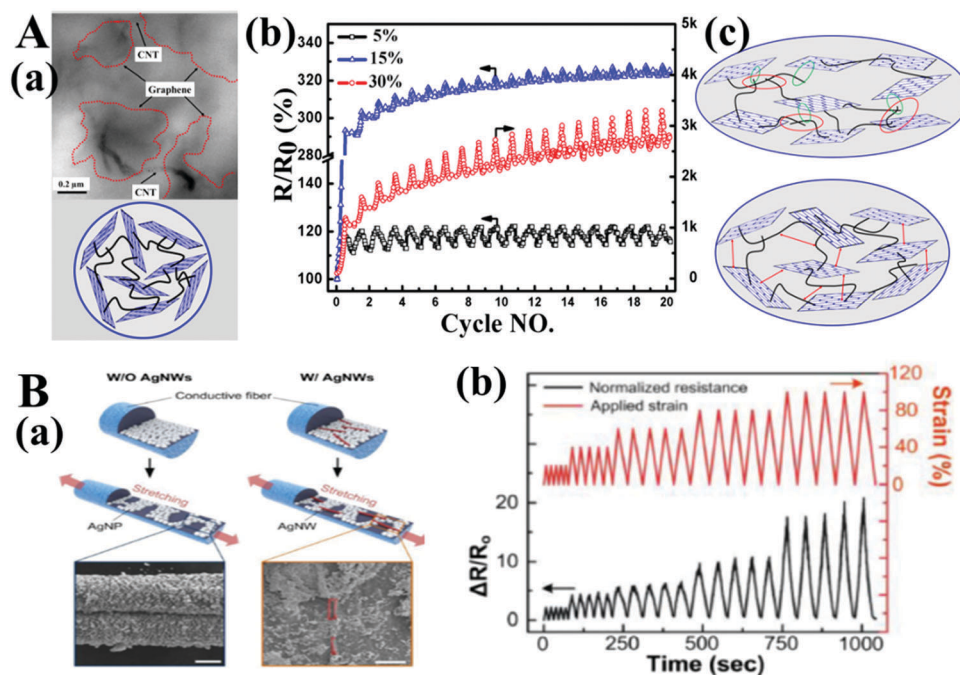


Fig. 4 (A) (a) TEM image and sketch of the synergistic effect between CNT and graphene; (b) response of sensor to cyclic loading at different strain; (c) sketch of the change of the hybrid conductive networks under larger and smaller strain (adapted with permission from ref. 66 Copyright 2016, Royal Society of Chemistry). (B) (a) Schematic illustration of changes in AgNWs and AgNP in the composite fiber at 50% strain; (b) response of sensor to cyclic loading at different strain (adapted with permission from ref. 10 Copyright 2015, Wiley-VCH Verlag GmbH & Co. KGaA, Weinheim).

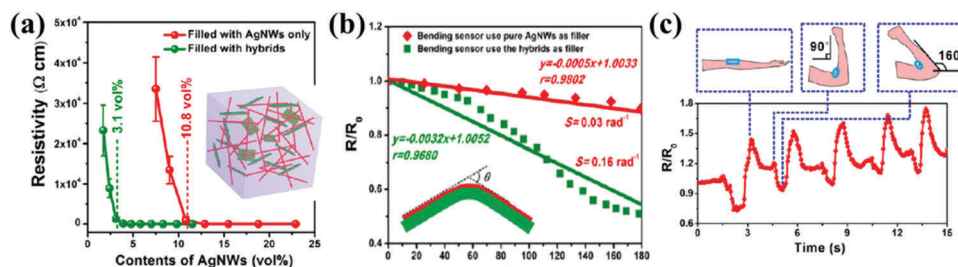


Fig. 5 (a) Percolation curve of AgNW/LDH/WPU and the sketch of the dispersion state of LDH and AgNW; (b) response of the sensor to bending cycle; (c) motion detection of the elbow joint (adapted with permission from ref. 134 Copyright 2015 American Chemical Society).

Wei and coworkers effectively implemented a homogeneous dispersion of AgNWs through the addition of 2D Co–Al layered double hydroxides (LDHs) in waterborne polyurethane (WPU) (Fig. 5a).<sup>134</sup> A significant decrease in the percolation threshold from 10.8 vol% to 3.1 vol% was achieved due to the existence of hydrogen bonding between them, weakening the depletion-induced interaction among the AgNWs. Meanwhile, a wearable bending sensor was fabricated by screen printing the AgNW/LDH/WPU conductive ink onto paper. Because of the separation effect of LDHs, the hybrid conductive network was easy to destruct compared to the condensed AgNW conductive network. Therefore, ECPCs filled with a hybrid filler possess higher sensitivity and liner fitting compared to ECPCs filled with AgNWs only (Fig. 5b). Meanwhile, it also showed excellent sensitivity toward various bending angles and showed extreme bending stability (Fig. 5c).

## 4 CPC-based strain sensors with special phase morphology design

In addition to the influence of the nanofiller's type and dimension on the sensing performance of ECPCs, special phase morphology design is another important fact to be generally considered.<sup>185</sup> The design of a micro/nanostructure has been implemented to achieve this goal, and it has been widely verified to be an effective measure in the field of functional polymer composites, including EMI shielding materials, hydrophobic materials, and energy storage materials. For ECPCs, phase morphology design is usually utilized to lower the percolation threshold. Also, its enhancement of the strain-sensing performance was also reported by lots of researchers, which will be discussed in detail in this part.

### 4.1 ECPCs with a segregated structure

Since the first publication about segregated structures in 1971,<sup>186</sup> lots of research works have been done on this issue. The so-called segregated structure in ECPCs means that the conductive fillers are mainly located at the interfaces between the polymeric matrix particles, applied using a mixing and hot-compression technique. This special structure is beneficial for the construction of an effective percolation network with a lower conductive filler loading. Compared with conventional ECPCs with a relatively dense distribution of conductive paths,

the special distribution state is easy to destruct upon external stress, causing a stable output signal and higher sensitivity.

For example, electrical-conductive PDMS/MWCNT composites with a segregated structure were obtained after a complete curing of a PDMS/MWCNT base/pre-cured PDMS particle mixture.<sup>187</sup> Fig. 6A(a) shows the SEM image of the prepared sample, where it can be seen clearly that the isolating phase pre-cured PDMS particles (highlighted by the red dotted line) were distributed homogeneously in the continuous PDMS/MWCNT phase, forming the segregated structure. In this study, conventional samples with 0.6 vol% MWCNTs and the self-segregated samples with 0.12 vol% MWCNTs possessed a stable conductive network and were thus chosen to investigate the influence of phase on the piezoresistive behaviors of ECPCs. As shown in Fig. 6A(b), a higher sensitivity was obtained for ECPCs with a segregated structure compared with the conventional samples. This interesting result was mainly ascribed to the PDMS particles having a higher modulus, generating a significant destruction towards the conductive networks located at their interspace compared with the conventional samples upon compression (Fig. 6A(c)). Besides, Wang *et al.* prepared NR/CNT composites using a latex assembly approach, and the segregated structure was successfully obtained with the assistance of CNC (Fig. 6B(a)).<sup>110</sup> In a comparison of the strain performances, shown in Fig. 6B(b), the segregated composites with 2.0 vol% CNT (CNT@CNC/NR-2.0) exhibited an abrupt response pattern and a GF value of 43.5 was estimated at a strain of up to 100%, but a relatively flat response was observed for the conventional sample with the same conductivity (CNT/NR-7.9). Meanwhile, it was found that the sensitivity decreased with increasing the CNT loading due to the high entanglement of CNT, which is not easy to be disrupted at the same strain. In addition, because the CNC rigid skeleton structure endowed the segregated conductive network with good resilience, almost full recoverability was obtained for all the segregated samples during the cyclic loading process, Fig. 6B(c).

### 4.2 ECPCs with a porous structure

Generally, the construction of a porous structure could effectively reduce the weight and enhance the compressibility of ECPCs. Besides, the conductive filler distributed on the 3D cell skeleton provides for a less densely percolated network, which helps to obtain a lower percolation threshold and enhanced



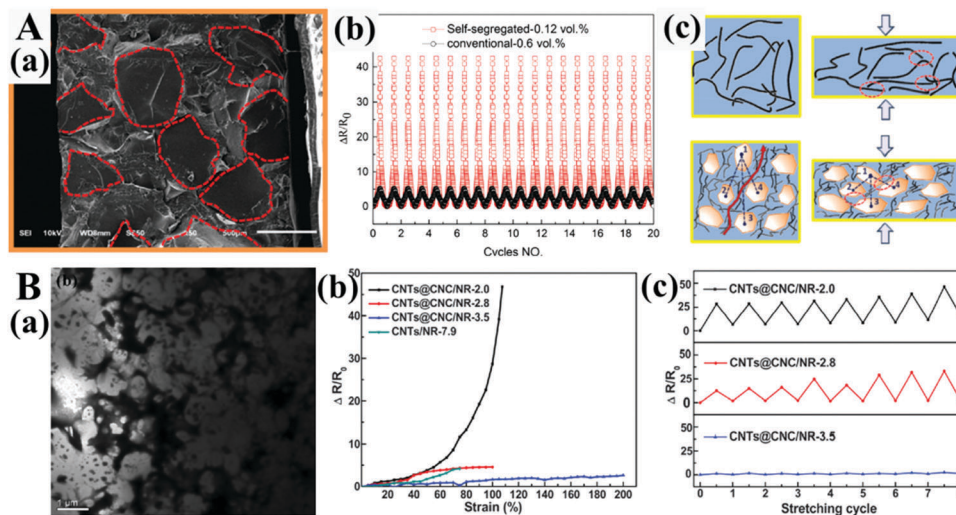


**Fig. 6** (A) (a) SEM image of segregated PDMS/CNT nanocomposites, the areas around the red dotted lines indicate the segregated PDMS particles; (b) response of the segregated sample and the conventional sample; (c) schematic of the damage model for conductive pathways in conventional samples and segregated samples under compression (adapted with permission from ref. 187 Copyright 2017, Royal Society of Chemistry). (B) (a) TEM image of CNT@CNC/NR nanohybrid aqueous suspension; (b) response of different samples during the tension process; (c) response of segregated samples to cyclic loading (adapted with permission from ref. 110 Copyright 2016, Royal Society of Chemistry).

sensitivity. Lots of related research works have been conducted by our group and other groups in this area.<sup>65,69,81,188–191</sup> For example, our group successfully prepared porous CNT/TPU and graphene/TPU nanocomposites using the thermally induced phase separation (TIPS) technique illustrated in Fig. 7a.<sup>65,69</sup> As shown in Fig. 7b, both TPU-based conductive foams possessed the characteristics of lightweight ( $0.1 \text{ g cm}^{-3}$ ) and ultrahigh compressibility (more than 90%). In addition, it could be seen that the type of conductive filler played an important role in the porous structure. Specifically, the addition of 1D CNT is beneficial for the formation of a complete and robust cell wall because of its entangled structure (Fig. 7c). However, some defects also existed on the cell wall of the porous graphene/TPU composites due to the flexibility of graphene (Fig. 7e). Therefore, the resistance of porous CNT/TPU exhibited a decreasing trend due to densification of the porous structure (Fig. 7d) during the compression procedure, and

an opposite piezoresistive behavior was observed caused by the breaking down of the defective cell wall (Fig. 7f). Finally, after stabilization of the cyclic loading, both porous ECPCs exhibited good recoverability and reproducibility upon cyclic compression over a wide strain of up to 90%.

In addition, the very simple and cost-efficient dip-coating strategy is another widely used technology to prepare porous ECPCs.<sup>72,192–194</sup> For example, Wu and coauthors fabricated porous conductive ECPCs by dipping commercial PU sponge into a suspension of CB with an opposite charge cyclically (Fig. 8a).<sup>193</sup> The resistance of the conductive sponge exhibited a trend of increase before decrease over a compression strain of up to 60% (Fig. 8b). Under a small strain amplitude (less than 9%), the formation of microcracks on the CB layer induced an increase in resistance. With a further increase in the strain, the neighboring cell walls contacted each other gradually, causing

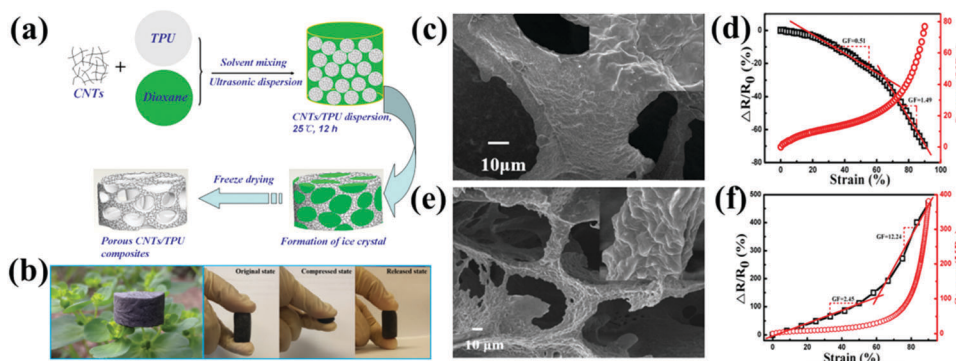


**Fig. 7** (a) Schematic for the fabrication of porous TPU based composites by TIPS technique; (b) digital images of ECPCs foam with 3 wt% graphene and the compression process; SEM of the cell strut of CPCs foam with (c) 0.51 vol% CNT and (e) 0.1 vol% graphene; piezoresistivity of ECPCs foam with (d) 0.51 vol% CNT and (f) 0.1 vol% graphene (adapted with permission from ref. 65 and 69 Copyright 2017, Royal Society of Chemistry. Copyright 2016, AIP Publishing).

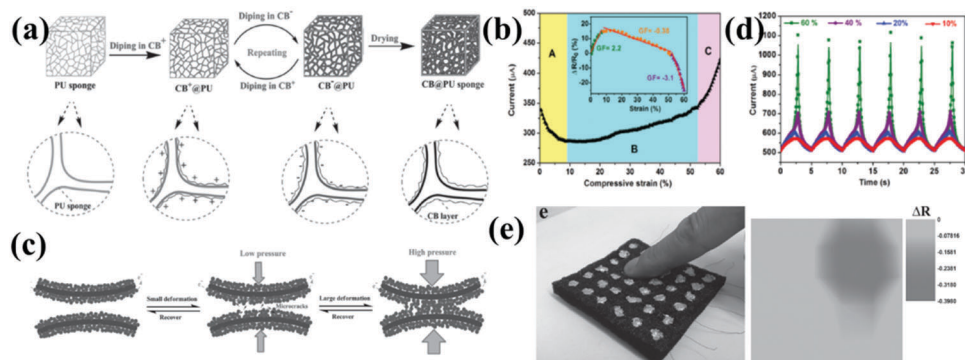


**Fig. 8** (a) Schematic diagram for the preparation of CB@PU sponges; (b) responsive current curve of a CB@PU sponge versus compressive strain along with the corresponding GF variation (inset); (c) schematic evolutions of the conductive pathways in a CB@PU sponge during continuous compressive deformation; (d) repeatedly compressing tests of a CB@PU sponge upon different strains; (e) index finger was pressed on the artificial electronic skin and the corresponding color contrast mapping (adapted with permission from ref. 193 Copyright 2016, Wiley-VCH Verlag GmbH & Co. KGaA, Weinheim).

a decrease in resistance (Fig. 8c). Overall, as shown in Fig. 8d, the conductive sponge exhibited good recoverability and reproducibly under cyclic compression, indicating its great potential to serve as an ideal piezoresistive sensor. When the ECPCs were fabricated into pressure-sensitive artificial electronic skin, the location and shape of an object could be detected simultaneously, showing great potential as an artificial intelligent sensor (Fig. 8e).

Recently, conductive aerogels have aroused researchers' wide interest due to their excellent characteristics, including lightweight, high porosity, and electrical conductivity.<sup>195–197</sup> They have been widely used in many fields, including supercapacitors, solar cells, and electrodes. Due to their limited compressibility, hybrid aerogel composites are usually prepared to serve as strain sensors. For example, Hu *et al.* used an infiltration–evaporation–curing technique to coat the graphene aerogel (GA) uniformly with a flexible PDMS layer (Fig. 9A(a)).<sup>198</sup>

The hybrid composites possessed excellent compressibility and recoverability at a strain of up to 90%, preventing the occurrence of surface cracks of the pure graphene aerogel. Hence, the compressive strength and Young's modulus of the pure graphene aerogel were also effectively enhanced. As a strain sensor, it exhibited stable and linear variation during compression cycles under various strain rates, showing good electromechanical stability (Fig. 9A(b)). As another example, Tang *et al.* successfully fabricated a lightweight robust and elastic CuNW conductive aerogel with the help of a trace amount of poly(vinyl alcohol) (Fig. 9B(a)).<sup>195</sup> Compared with pure CuNW aerogel, typical elastic deformation was observed for the hybrid CuNW aerogel from the stress–strain curve, endowing it with good recoverability under a compression strain of up to 60% (Fig. 9B(b)). Meanwhile, the hybrid aerogel showed a stable and reversible sensing behavior under different compression stresses (Fig. 9B(c)).

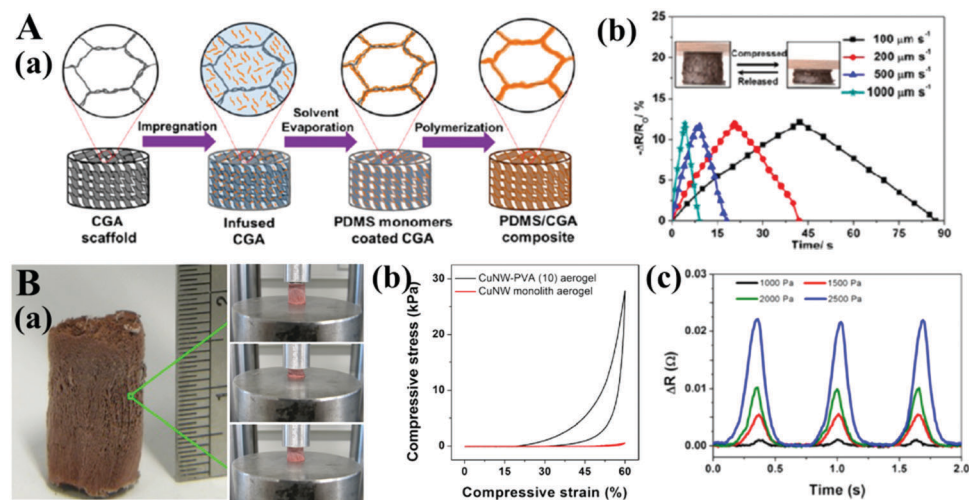


**Fig. 9** (A) (a) Schematic illustration of the fabrication process of PDMS/GA; (b) resistance change of PDMS/GA with strain up to 50% at different compression rates, digital photo of the cyclic compression process (inset) (adapted with permission from ref. 198 Copyright 2014 American Chemical Society). (B) (a) Photographic image of CuNW–PVA hybrid aerogel with good elasticity; (b) compressive stress–strain curves of the hybrid aerogel and CuNW monolith aerogels under a compressive strain of 60%; (c) response of the hybrid aerogel to cyclic compression test (adapted with permission from ref. 195 Copyright 2014 American Chemical Society).

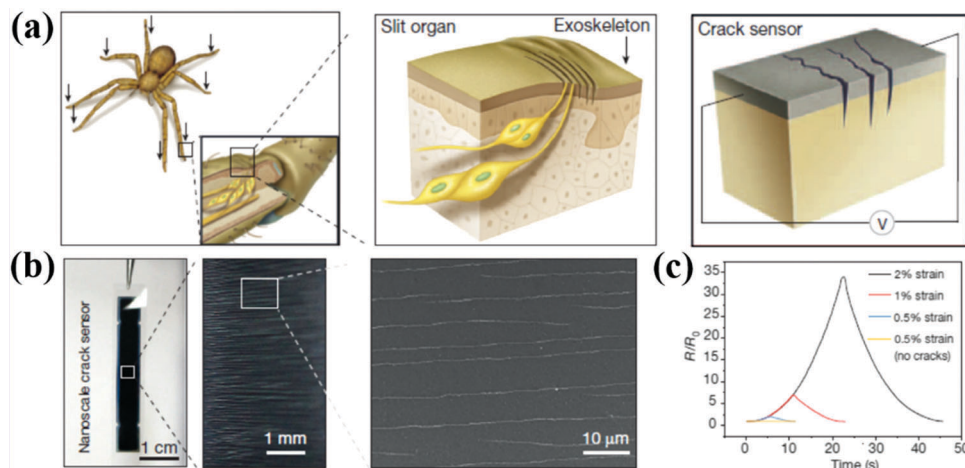


Fig. 10 (a) Schematic illustrations of an ultra-mechanosensitive nanoscale crack junction-based sensor inspired by the spider sensory system; (b) left, image of the spider-inspired sensor with a cracked; right, enlarged image of the cracks in the surface of the sensor in the left-hand image; SEM image of the boxed region of the left-hand image; (c) reversible loading–unloading behavior for various final strains (adapted with permission from ref. 149 Copyright 2014 Springer Nature).

### 4.3 ECPCs with a microcrack structure

Since the first research about the crack-based ECPCs strain sensor conducted by Kang and coworkers in 2014,<sup>149</sup> it has attracted widespread attention in the field.<sup>16,118,131,138,191,199–206</sup> The design of ECPCs with a microcrack structure is inspired by the spiders' crack-shaped slit organs on their legs, which can detect small external force variations, whereby the opening and closure between the cracks distributed in the conductive layer would generate a significant resistance variation signal, endowing the ECPCs with ultrasensitive strain detection ability and high strain sensitivity (Fig. 10a). In the study, polyurethane acrylate was covered with a layer of Pt film, and controlled cracks were generated in the Pt film through mechanical bending under different radii of curvature (Fig. 10b). Compared with the ECPCs without a microcrack, the cracked sample exhibited ultrasensitive strain detection ability even at a strain amplitude as low as 0.5%, and a 450-fold higher resistance variation was observed (Fig. 10c). As for the GF of the cracked sample, the highest value of about 2079 was obtained.

Inspired by this, Chen *et al.* obtained AgNW/graphene hybrid particles by assembly due to the existence of hydrogen-bonding interactions between AgNWs and GO nanosheets.<sup>90</sup> Because of the particles' point-to-point connections and weak interactions between them, the hybrid particle layer was easily broken upon external stress, causing a microcrack structure. In their study, TPU solution was cast onto the hybrid particle layer to achieve a flexible strain sensor. As shown in Fig. 11A(a), a cracked and overlapping structure was observed for the composites after 10% prestretching, whereby the crack-based sensor possessed a GF as high as 20 ( $\Delta\varepsilon < 0.3\%$ ), 1000 ( $0.3\% < \Delta\varepsilon < 0.5\%$ ), and 4000 ( $0.8\% < \Delta\varepsilon < 1\%$ ). In addition, it could be seen that larger prestretching leads to a wider working range, but the GF of the composites under 1% strain was also reduced (Fig. 11A(b)). For its practical application, as seen in Fig. 11A(c), the composites exhibited an accurate and stable response for cyclic tests under different

strains. Recently, due to the many excellent properties (including flexibility, recyclability, low cost, and degradability around the environment) of paper, paper-based electronic devices have attracted extensive attention. Hence, Liu and coworkers prepared a flexible cracked paper-based sensor by dip-coating in an aqueous suspension of CB and carboxymethyl cellulose (Fig. 11B(a)), and lots of cracks with a width of 10–20  $\mu\text{m}$  were observed (Fig. 11B(b)).<sup>207</sup> Based on the special structure, the sensor exhibited a high GF of about 4.3 under 0.6% strain amplitude. Besides, it also showed excellent durability and stability under 0.24% strain during 1000 cycles, and a relatively shorter responsive time (approximately 0.24 s) was observed (Fig. 11B(c)).

### 4.4 ECPCs with a wrinkled structure

For ECPCs, a wrinkled structure could effectively provide strain relief during the tensile procedure, enhancing the stretchability of ECPCs significantly. Therefore, the construction of a special structure turned to be another useful method to improve the property of ECPC-based strain sensors.

Based on the mismatches in stiffness between the conductive layer and polymer matrix, the special wrinkled structure is usually formed during the release process of the pre-stretched ECPCs<sup>205</sup> or the thermal shrinking process of the polymer matrix.<sup>6,13</sup> For example, Park and coworkers prepared a wrinkled CNT thin film *via* heat-induced biaxial shrinking on a shape-memory polystyrene matrix; then the wrinkled CNT thin film was transferred to soft Ecoflex to constitute wrinkled CNT-Ecoflex (wCE) strain sensors (Fig. 12A(a)).<sup>6</sup> During the tension process, as seen in Fig. 12A(b), the neighboring contacted CNT wrinkles were slowly separated from each other and aligned in the direction of the load, enabling the sensor to be sensitive under a strain up to about 750% (Fig. 12A(c)), which was about a 60-fold increase in stretchability compared with the planar CNT films. Besides, it also exhibited good reproducibility under cyclic strains between 0 and 300% (Fig. 12A(d)). All these

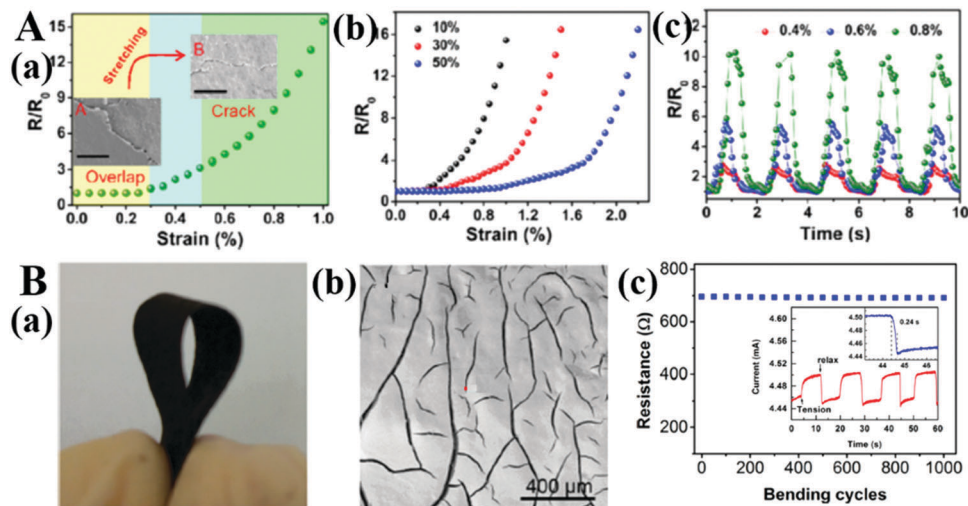


**Fig. 11** (A) (a) Resistance variation of AgNW/graphene/TPU composites to 1% strain after 10% stretching, inset a and b are SEM images of the surface before and after stretch (0.8% strain); (b) the working range dependent on the prestretching level; (c) cyclic test of the composites for various strains (adapted with permission from ref. 112 Copyright 2016 American Chemical Society). (B) (a) Photographs and (b) SEM of CB coated paper; (c) resistance of the sensor during 1000 bending–unbending cycles. The inset curve is the response curve of the sensor under 0.24% tension strain after 1000 bending–unbending cycles (adapted with permission from ref. 207 Copyright 2017 American Chemical Society).

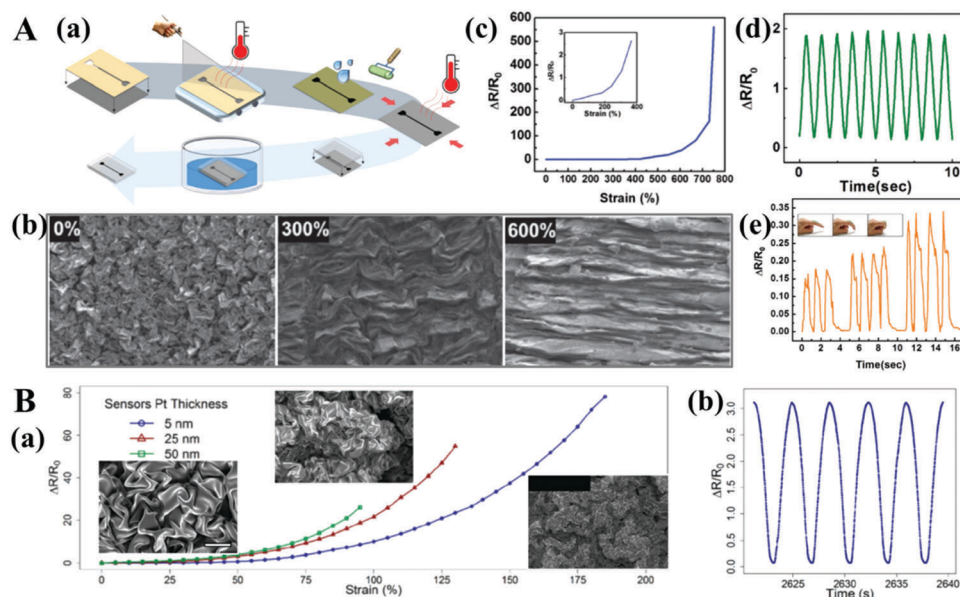


**Fig. 12** (A) (a) Fabrication process of wrinkled CNT-Ecoflex strain sensor; (b) SEM images of the morphology of wrinkled CNT thin film at different strains; (c) relative change in resistance vs. strain on wrinkled CNTs on Ecoflex substrate (the inset plot is an expanded view of 0–400% strain); (d) relative change in resistance for cyclic strain between 0 and 300%; (e) relative change in resistance while bending the strain sensor at joint area of finger (adapted with permission from ref. 6 Copyright 2016, Wiley-VCH Verlag GmbH & Co. KGaA, Weinheim). (B) (a) The strain sensitivity of the best performing 5, 25, and 50 nm wPt strain sensors (the inset plot is SEM of Pt thin films at 5, 25, and 50 nm); (b) a small subset of strain cycling to show the repeatability and stability of the sensor (adapted with permission from ref. 13 Copyright 2016, Royal Society of Chemistry).

endowed the sensor with excellent potential and applicability to serve as a wearable physiological monitoring device (Fig. 12A(e)). Meanwhile, the same group also fabricated a flexible wrinkled platinum (wPt) strain sensor using the same preparation technology.<sup>13</sup> As shown in Fig. 12B(a), the wrinkle density could be tuned through changing the thickness of the platinum layer. A thinner platinum layer is beneficial for the formation of a

high-density wrinkle structure, endowing the sensor with more strain relief and an increase in the strain sensor range. This means that the dynamic range and sensitivity of the wrinkled structured strain sensor could be effectively tuned by changing the conductive layer thickness. Finally, stable and reversible sensing behavior was also obtained under 50% strain for the 5 nm wPt sensor (Fig. 12B(b)).

## 5 Imperative features for ECPC-based strain sensors

In order to enlarge their usage scope, especially in the fields of wearable electronics and human health monitoring, several imperative features are needed to be considered and addressed for ECPC-based strain sensors. All these will be highlighted in this part, with an aim to provide some valuable suggestions.

### 5.1 Self-healing capability

During the long-term using process, ECPC-based strain sensors generally tend to become invalid and unstable due to the unrecoverable destruction of the conductive network upon mechanical deformation or accidental damage. Hence, a self-healing capability is essential to enhance ECPCs' durability as strain sensors and to prolong their lifetime in practical application.

To date, self-healing electronic materials have mainly been fabricated using two different methods. One method mainly refers to the microencapsulation method, which releases the healing agent to repair the destructed conductive network. For example, Liu and coauthors fabricated self-healing ECPCs by mixing the hybrids of poly(3-caprolactone) (PCL), graphene

oxide, and AgNW with PDMS.<sup>176</sup> As shown in Fig. 13A(a), when the scratched sample was set at the healing temperature of 80 °C, the low melting point PCL melted and flowed into small voids with the conductive filler, reconstructing new conductive networks. As a result, the healed sample exhibited good conductive stability and sensitivity during the cyclic bending process (Fig. 13A(b)), and the healing efficiency of conductivity was observed to be 65% after 3 healing cycles (Fig. 13A(c)).

Another method is the addition of a conductive filler into the intrinsic self-healing materials, making the composites recover to their initial state based on reversible covalent bonds, non-covalent bonds, and hydrogen bonds. For instance, Wang *et al.*<sup>208</sup> synthesized a stretchable ternary polymer using polyaniline, polyacrylic acid, and phytic acid. It is known that dynamic hydrogen bonding and electrostatic interactions can dynamically associate and disassociate at room temperature, so the cut samples could contact each other tightly under mild pressure and successfully self-heal in a 24 h healing period (Fig. 13B(a)). In addition, the healed sample possessed almost the same mechanical properties as the initial samples (Fig. 13B(b)). Comparing the GF of the original and healed strain sensor in Fig. 13B(c), there is almost no GF variation

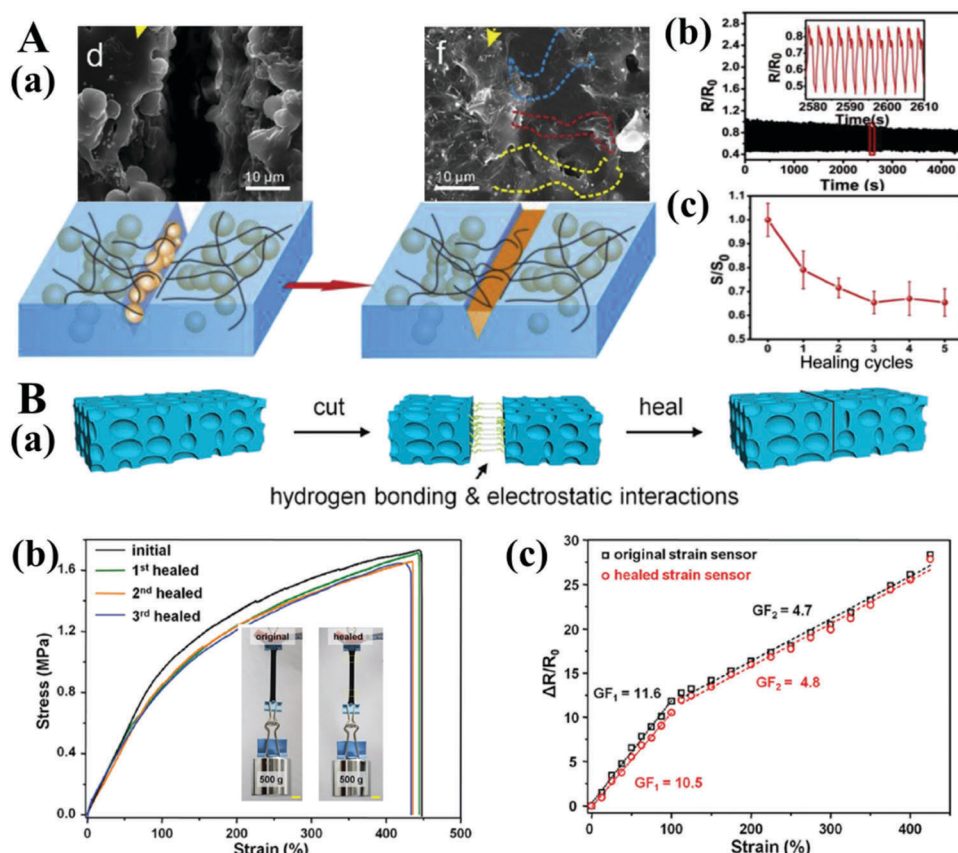


**Fig. 13** (A) (a) SEM images and schematic illustration of the self-healing process of the strain sensor at 80 °C; (b) responses of the healed strain sensors to bending cycles (bending down, maximum angle 90°, after handled at 80 °C for 3 min); (c) variation of conductivity ( $S$ ) as a function of healing cycles (adapted with permission from ref. 176 Copyright 2017, Elsevier). (B) (a) Schematic illustration of the self-healing process due to hydrogen bonding and electrostatic interactions; (b) stress–strain curves of the polymer film after multiple breaking/healing cycles (the inset plot is the self-healed polymer film can completely support  $\approx 500$  g mass. Yellow rectangles indicate the wound/healing points in the polymer film); (c) gauge factors measured as a function of applied strains (adapted with permission from ref. 208 Copyright 2018, Wiley-VCH Verlag GmbH & Co. KGaA, Weinheim).

below and exceeding 100% strain within a maximal strain of up to 425%, thus showing excellent self-healing capability.

## 5.2 Superhydrophobicity

Superhydrophobicity is another urgent characteristic to be considered for the design of ECPCs as strain sensors for use in extreme working conditions, because the existence of water tends to cause the deterioration of electronic devices. Hence, the fabrication of a strain sensor with good superhydrophobicity is a big challenge. Generally, the construction of a micro-nano rough structure on the surface of a sample is the most commonly used method to obtain superhydrophobic materials. However, the deformation of such a superhydrophobic material usually leads to the destruction of the micro-nano rough structure, reducing the hydrophobicity of materials. Accordingly, it is of great value to construct extremely stable superhydrophobic structure for severe deformation.

To achieve this goal, as shown in Fig. 14a, Li *et al.* fabricated an electrical thermoplastic elastomer (TPE)-based coating with superhydrophobic micrometer-sized features by spray-coating a CNT/cyclohexane suspension, followed by treatment with ethanol.<sup>209</sup> Here, the spraying speed was controlled to balance the spraying and solvent evaporation time to construct perfect micrometer-sized features, and the ethanol was applied to dissolve the TPE matrix to form the pit-like features. As for its superhydrophobicity upon external strain, it can be seen in Fig. 14b that the contact angle (CA) effectively remained above 150° up to a strain of 50%, indicating good durability and stability of the superhydrophobicity. During the cyclic stretching between 0–50% at different frequencies, the sensor showed highly reproducible sensing behavior (Fig. 14c), indicating great potential for the detection of human activities with different frequencies. In addition, within a strain range of 0–5%, the sensor also exhibited a much faster response time of 8 ms than that reported in other publication (Fig. 14d).

Meanwhile, Su and coauthors also sprayed a prestretched natural rubber (NR) substrate with the hybrids of a hydrophobic 1-octadecanethiol-modified silver nanoparticles

(M-AgNPs)/SEBS suspension.<sup>210</sup> As shown in Fig. 15a, during the spraying process, lots of protuberances appeared due to the aggregation of M-AgNPs in the SEBS matrix. Then, the protuberances tended to be compressed arising from the contraction force of the SEBS matrix when the prestrained NR strip was released, forming a micrometer-sized rough hydrophobic surface (Fig. 15b). When the sample was stretched to different stretch ratios ( $\lambda$ ,  $1 \leq \lambda \leq 9$ ), almost no obvious changes in contact angle (CA) and sliding angle (SA) were observed, indicating excellent preservation of the superhydrophobicity under extreme tension deformation (Fig. 15c). During cyclic stretching at  $\lambda = 3$ , its CA also kept above 150° after 500 cycles, showing a good durability of the superhydrophobicity (Fig. 15d).

## 5.3 Good light transmission

Form an aesthetic point of view, good imperceptibility is very necessary for a strain sensor to be fixed at the face, nose, or other parts of human body during daily activities, so high optical transparency needs to be satisfied for such ECPC-based strain sensors. However, due to the fact that a high loading of conductive filler is usually needed for the fabrication of ECPCs, most ECPCs exhibit nontransparency. To improve the transparency of ECPCs, many related investigations have been conducted and ECPCs with excellent transparency and strain-sensing performance have been successfully obtained, providing significant guidelines for the fabrication of invisible wearable electronics.<sup>15,63,211,212</sup>

For example, Roh *et al.* prepared a transparent sandwich-like stacked nano-hybrid film by spray-coating an elastic PU-PEDOT:PSS layer and CNT layer onto an O<sub>2</sub> plasma-treated PDMS layer by layer (Fig. 16A(a)).<sup>15</sup> In this study, the influence of CNT concentration on the transparency and strain-sensing performance was investigated. Compared with the sample with lower CNT concentration of 1 and 3 mg mL<sup>-1</sup>, the sample with a higher CNT concentration (5 mg mL<sup>-1</sup>) exhibited a stable strain-sensing behavior and lower sensitivity (Fig. 16A(b)) under different cyclic bending strains. As for the transparency shown in Fig. 16A(c), a higher CNT concentration led to the reduction of transparency, but the sample with

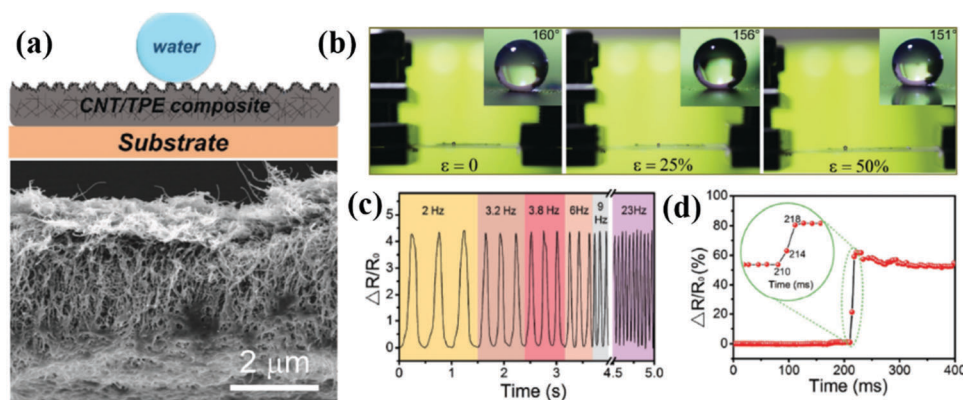


**Fig. 14** (a) Schematic illustration of the MWCNT/TPE composite film coatings and SEM image of the film's cross-section treated with ethanol for 2 min; (b) optical photographs of water droplets on the film with different tensile strains. Insets: CA angle optical image; (c) resistance variation under repetitive stretching from  $\varepsilon = 0\%$  to  $\varepsilon = 50\%$  with different frequencies; (d) time response of the sensor upon applying strain from  $\varepsilon = 0\%$  to  $\varepsilon = 5\%$  (adapted with permission from ref. 209 Copyright 2017, Wiley-VCH Verlag GmbH & Co. KGaA, Weinheim).

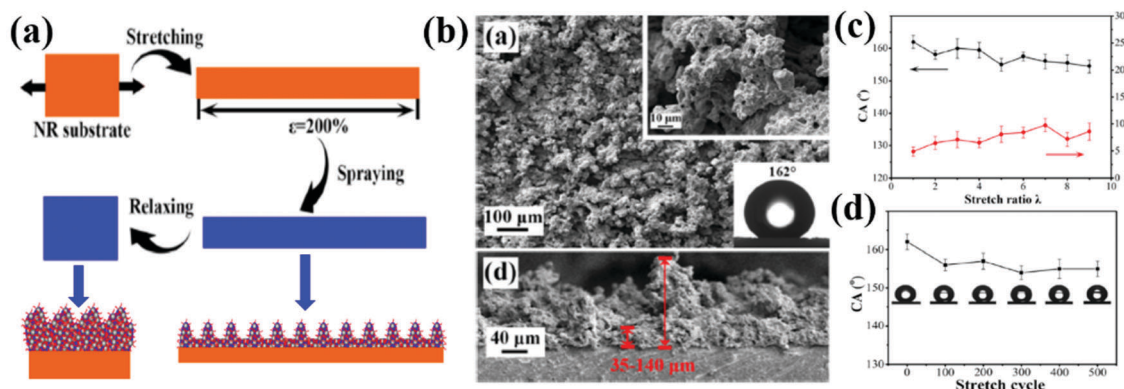


Fig. 15 (a) Schematic illustration of the fabrication of conductive superhydrophobic coating on the NR strip; (b) SEM images of the conductive superhydrophobic coatings fabricated at  $\varepsilon = 200\%$  and the corresponding cross-sectional images. Insets: CA optical image; (c) CA and SA of the superhydrophobic coating at different  $\lambda$ ; (d) CA change of the superhydrophobic coating with stretching–relaxation cycles at  $\lambda = 3$  (adapted with permission from ref. 210 Copyright 2018 American Chemical Society).

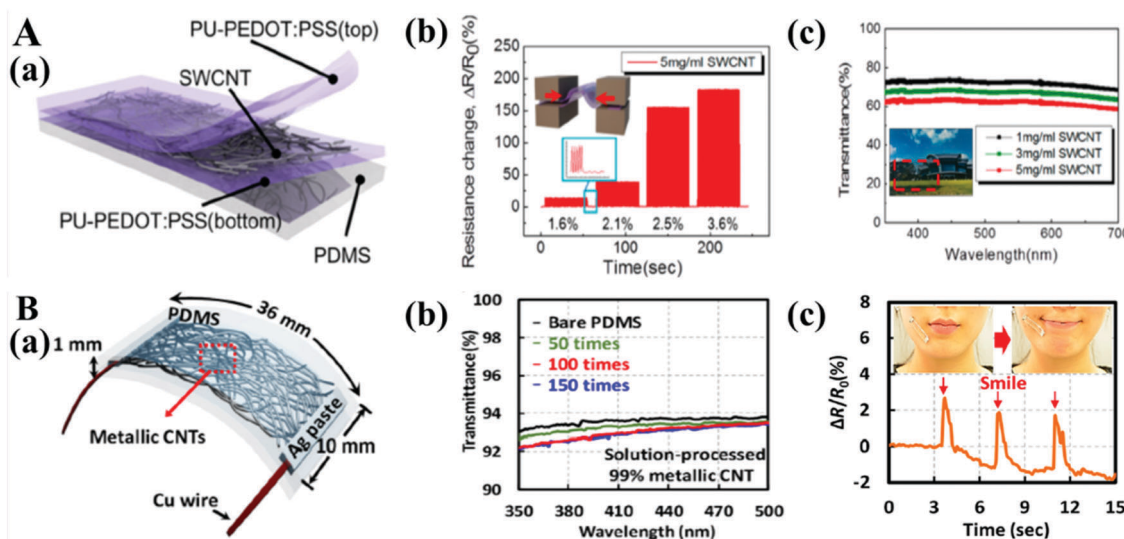


Fig. 16 (A) (a) Schematic illustration of the cross-section of the sandwich-like stacked PU-PEDOT:PSS/SWCNT/PU-PEDOT:PSS/PDMS sensor; (b) cyclic bending response of the sensor based on CNT concentration of  $5 \text{ mg mL}^{-1}$  to different strains; (c) optical transmittance of the sensor based on with different CNT concentrations in the visible range. Inset is the photograph of the sandwich-like sensor (adapted with permission from ref. 15 Copyright 2015 American Chemical Society). (B) (a) Schematic illustration of the transparent CNT–PDMS composite strain sensor in the form of a sandwich structure; (b) optical transparency of the sensor with different number of sprays in the visible range; (c) applications of the transparent sensor to the detection of smiling motion (adapted with permission from ref. 63 Copyright 2017 American Chemical Society).

$5 \text{ mg mL}^{-1}$  CNT concentration still could supply enough optical transparency (62%) in the visible wavelength range to fulfill the practical requirement.

Similarly, Lee *et al.* used the spray-coating technique to deposit 99% metallic CNT solution ( $0.01 \text{ mg mL}^{-1}$ ) onto flexible  $\text{O}_2$  plasma-treated PDMS to fabricate a sandwich-structured CNT–PDMS sensor with high optical transparency (Fig. 16B(a)).<sup>63</sup> It can be found in Fig. 16B(b) that the transparency still kept over 92% even for sample with as high as 150 CNT sprays, which benefited from the highly purified, solution-processed CNTs used in this study. In addition, the transparent sensor could be used for the detection of various human activities and emotions (*e.g.*, finger joint motion, elbow joint motion, swallowing motion, and smiling), showing

excellent distinguishable responses. Take the smiling motion for example, as shown in Fig. 16B(c), the transparent sensor exhibited accurate response and almost full recovery under cyclic motion, showing great potential for the fruitful implementation of skin-mountable electronic devices.

## 6 Conclusions and outlook

Electrically conductive polymer composites serving as smart flexible strain sensors have received great attention due to their wide working strain gauge, high sensitivity, and good reproductivity after repetitive usage. According to the response mechanism, the sensing performances of ECPC-based strain

sensors could be tuned by changing the conductive fillers' type, structure, and loading. Meanwhile, morphology design of the conductive network in ECPCs is another important tool to acquire a high-performance strain sensor with highly sensitive and resilient characteristics, especially for the detection of extremely small variations with significant sensitivity. Recently, in order to meet practical needs, ECPCs with imperative features, including self-healing capability, superhydrophobicity, good light transmission, have become enthusiastic research topics for many researchers. As a consequence, ECPCs are considered as an ideal substitute for conventional metal/inorganic semiconductor-based strain sensors, showing great potential to be used for the fabrication of wearable electronic devices. Although so many investigations about ECPC-based strain sensors have been conducted, there is still a lot to be done to promote their development.

## Conflicts of interest

There are no conflicts to declare.

## Acknowledgements

The authors gratefully acknowledge the financial support of this work by National Natural Science Foundation of China (Contract Number: 51803191, 11572290, 11432003), the National Key Research and Development Program of China (2016YFB0101602). H. Liu appreciate the start-up fund from Zhengzhou University.

## References

- X. Wu, Y. Han, X. Zhang and C. Lu, *ACS Appl. Mater. Interfaces*, 2016, **8**, 9936–9945.
- Y. Wang, L. Wang, T. Yang, X. Li, X. Zang, M. Zhu, K. Wang, D. Wu and H. Zhu, *Adv. Funct. Mater.*, 2014, **24**, 4666–4670.
- G.-H. Lim, N.-E. Lee and B. Lim, *J. Mater. Chem. C*, 2016, **4**, 5642–5647.
- C. S. Boland, U. Khan, C. Backes, A. O'Neill, J. McCauley, S. Duane, R. Shanker, Y. Liu, I. Jurewicz, A. B. Dalton and J. N. Coleman, *ACS Nano*, 2014, **8**, 8819–8830.
- J. J. Park, W. J. Hyun, S. C. Mun, Y. T. Park and O. O. Park, *ACS Appl. Mater. Interfaces*, 2015, **7**, 6317–6324.
- S.-J. Park, J. Kim, M. Chu and M. Khine, *Adv. Mater. Technol.*, 2016, **1**, 1600053.
- Z. Wang, Y. Huang, J. Sun, Y. Huang, H. Hu, R. Jiang, W. Gai, G. Li and C. Zhi, *ACS Appl. Mater. Interfaces*, 2016, **8**, 24837–24843.
- T. Yamada, Y. Hayamizu, Y. Yamamoto, Y. Yomogida, A. Izadi-Najafabadi, D. N. Futaba and K. Hata, *Nat. Nanotechnol.*, 2011, **6**, 296–301.
- X. G. Yu, Y. Q. Li, W. B. Zhu, P. Huang, T. T. Wang, N. Hu and S. Y. Fu, *Nanoscale*, 2017, **9**, 6680–6685.
- S. Lee, S. Shin, S. Lee, J. Seo, J. Lee, S. Son, H. J. Cho, H. Algadi, S. Al-Sayari, D. E. Kim and T. Lee, *Adv. Funct. Mater.*, 2015, **25**, 3114–3121.
- Y. Zheng, Y. Li, K. Dai, Y. Wang, G. Zheng, C. Liu and C. Shen, *Compos. Sci. Technol.*, 2018, **156**, 276–286.
- Y. Wang, J. Hao, Z. Huang, G. Zheng, K. Dai, C. Liu and C. Shen, *Carbon*, 2018, **126**, 360–371.
- J. D. Pegan, J. Zhang, M. Chu, T. Nguyen, S. J. Park, A. Paul, J. Kim, M. Bachman and M. Khine, *Nanoscale*, 2016, **8**, 17295–17303.
- J.-W. Zha, W. Huang, S.-J. Wang, D.-L. Zhang, R. K. Y. Li and Z.-M. Dang, *Adv. Mater. Interfaces*, 2016, **3**, 1500418.
- E. Roh, B. U. Hwang, D. Kim, B. Y. Kim and N. E. Lee, *ACS Nano*, 2015, **9**, 6252–6261.
- L. Yi, W. Jiao, K. Wu, L. Qian, X. Yu, Q. Xia, K. Mao, S. Yuan, S. Wang and Y. Jiang, *Nano Res.*, 2015, **8**, 2978–2987.
- (a) C. Yan, J. Wang, W. Kang, M. Cui, X. Wang, C. Y. Foo, K. J. Chee and P. S. Lee, *Adv. Mater.*, 2014, **26**, 2022–2027; (b) Y. Tang, Z. Zhao, H. Hu, Y. Liu, X. Wang, S. Zhou and J. Qiu, *ACS Appl. Mater. Interfaces*, 2015, **7**, 27432–27439; (c) B. Song, T. Wang, H. Sun, Q. Shao, J. Zhao, K. Song, L. Hao, L. Wang and Z. Guo, *Dalton Trans.*, 2017, **46**, 15769–15777; (d) X. Lou, C. Lin, Q. Luo, J. Zhao, B. Wang, J. Li, Q. Shao, X. Guo, N. Wang and Z. Guo, *ChemElectroChem*, 2017, **4**, 3171–3180.
- (a) H. Du, C. Zhao, J. Lin, Z. Hu, Q. Shao, J. Guo, B. Wang, D. Pan, E. K. Wujcik and Z. Guo, *Chem. Rec.*, 2018, **18**, 1365–1372; (b) Z. Sun, *et al.*, *CrystEngComm*, 2017, **19**, 3288–3298; (c) L. Zhang, W. Yu, C. Han, J. Guo, Q. Zhang, H. Xie, Q. Shao, Z. Sun and Z. Guo, *J. Electrochem. Soc.*, 2017, **164**, H651–H656; (d) L. Zhang, M. Qin, W. Yu, Q. Zhang, H. Xie, Z. Sun, Q. Shao, X. Guo, L. Hao, Y. Zheng and Z. Guo, *J. Electrochem. Soc.*, 2017, **164**, H1086–H1090; (e) Y. Zhang, L. Qian, W. Zhao, X. Li, X. Huang, X. Mai, Z. Wang, Q. Shao, X. Yan and Z. Guo, *J. Electrochem. Soc.*, 2018, **165**, H510–H516.
- (a) M. Amjadi, A. Pichitpajongkit, S. Lee, S. Ryu and I. Park, *ACS Nano*, 2014, **8**, 5154–5163; (b) C. Lin, H. Hu, C. Cheng, K. Sun, X. Guo, Q. Shao, J. Li, N. Wang and Z. Guo, *Electrochim. Acta*, 2018, **260**, 65–72; (c) Q. Hou, J. Ren, H. Chen, P. Yang, Q. Shao, M. Zhao, X. Zhao, H. He, N. Wang, Q. Luo and Z. Guo, *ChemElectroChem*, 2018, **5**, 726–731.
- R. Rahimi, M. Ochoa, W. Yu and B. Ziaie, *ACS Appl. Mater. Interfaces*, 2015, **7**, 4463–4470.
- (a) S. Chen, Y. Wei, X. Yuan, Y. Lin and L. Liu, *J. Mater. Chem. C*, 2016, **4**, 4304–4311; (b) Z. Zhao, R. Guan, J. Zhang, Z. Zhao and P. Bai, *Acta Metall. Sin. (Engl. Lett.)*, 2017, **30**, 66–72; (c) Z. Zhao, P. Bai, R. Guan, V. Murugadoss, H. Liu, X. Wang and Z. Guo, *Mater. Sci. Eng., A*, 2018, **734**, 200–209; Y. Zhao, L. Qi and Y. Jin, *et al.*, *J. Alloys Compd.*, 2015, **647**, 1104–1110; (d) Y. Zhao, S. Deng, H. Liu, J. Zhang, Z. Guo and H. Hou, *Comput. Mater. Sci.*, 2018, **154**, 365–370; (e) B. Kirubasanakar, V. Murugadoss, J. Lin, M. Dong, J.-X. Zhang, T. Li, N. Wang, Z. Guo, T. Ding, H. Liu and S. Angaiah, *Nanoscale*, 2018, DOI: 10.1039/c8nr06345a.



- 22 Y. Lin, S. Liu, S. Chen, Y. Wei, X. Dong and L. Liu, *J. Mater. Chem. C*, 2016, **4**, 6345–6352.
- 23 (a) Y. Guo, G. Xu, X. Yang, K. Ruan, T. Ma, Q. Zhang, J. Gu, Y. Wu, H. Liu and Z. Guo, *J. Mater. Chem. C*, 2018, **6**, 3004–3015; (b) W. Yu, C. Liu, L. Qiu, P. Zhang, W. Ma, Y. Yue, H. Xie and L. Larkin, *Eng. Sci.*, 2018, **2**, 1–3; (c) H. Gu, H. Zhang, J. Lin, Q. Shao, D. P. Young, L. Sun, T. D. Shen and Z. Guo, *Polymer*, 2018, **143**, 324–330; (d) H. Gu, H. Zhang, C. Gao, C. Liang, J. Gu and Z. Guo, *ES Mater. Manuf.*, 2018, DOI: 10.30919/esmm5f108.
- 24 C. Wang, Z. He, X. Xie, X. Mai, Y. Li, T. Li, M. Zhao, C. Yan, H. Liu, E. K. Wujcik and Z. Guo, *Macromol. Mater. Eng.*, 2018, **303**, 1700462.
- 25 J. Gu, W. Dong, Y. Tang, Y. Guo, L. Tang, J. Kong, S. Tadakamalla, B. Wang and Z. Guo, *J. Mater. Chem. C*, 2017, **5**, 6929–6936.
- 26 W. Zhao, J. Kong, H. Liu, Q. Zhuang, J. Gu and Z. Guo, *Nanoscale*, 2016, **8**, 19984–19993.
- 27 (a) Y. Pan, X. Liu, J. Kaschta, X. Hao, C. Liu and D. W. Schubert, *Polymer*, 2017, **113**, 34–38; (b) H. Wu, X. Huang and L. Qian, *Eng. Sci.*, 2018, **2**, 17–25.
- 28 Y. Gao, Q. Wang, J. Wang, L. Huang, X. Yan, X. Zhang, Q. He, Z. Xing and Z. Guo, *ACS Appl. Mater. Interfaces*, 2014, **6**, 5094–5104.
- 29 Q. He, T. Yuan, X. Yan, D. Ding, Q. Wang, Z. Luo, T. D. Shen, S. Wei, D. Cao and Z. Guo, *Macromol. Chem. Phys.*, 2014, **215**, 327–340.
- 30 X. Zhang, Q. He, H. Gu, H. A. Colorado, S. Wei and Z. Guo, *ACS Appl. Mater. Interfaces*, 2013, **5**, 898–910.
- 31 Y. Feng, X. Li, X. Zhao, Y. Ye, X. Zhou, H. Liu, C. Liu and X. Xie, *ACS Appl. Mater. Interfaces*, 2018, **10**, 21628–21641.
- 32 (a) P. Xie, Z. Wang, Z. Zhang, R. Fan, C. Cheng, H. Liu, Y. Liu, T. Li, C. Yan, N. Wang and Z. Guo, *J. Mater. Chem. C*, 2018, **6**, 5239–5249; (b) J. Wang, Z. Shi, X. Wang, X. Mai, R. Fan, H. Liu, X. Wang and Z. Guo, *Eng. Sci.*, 2018, DOI: 10.30919/es8d759; (c) X. Wang, X. Zeng and D. Cao, *Eng. Sci.*, 2018, **1**, 55–63; (d) L. Yan, H. Wang, D. Huang and H. Luo, *Eng. Sci.*, 2018, **1**, 4–20.
- 33 (a) K. Sun, R. Fan, X. Zhang, Z. Zhang, Z. Shi, N. Wang, P. Xie, Z. Wang, G. Fan, H. Liu, C. Liu, T. Li, C. Yan and Z. Guo, *J. Mater. Chem. C*, 2018, **6**, 2925–2943; (b) L. Wang, H. Qiu, C. Liang, P. Song, Y. Han, Y. Han, J. Gu, J. Kong, D. Pan and Z. Guo, *Carbon*, 2019, **141**, 506–514.
- 34 B. Qiu, J. Guo, Y. Wang, X. Wei, Q. Wang, D. Sun, M. A. Khan, D. P. Young, R. O'Connor, X. Huang, X. Zhang, B. L. Weeks, S. Wei and Z. Guo, *J. Mater. Chem. C*, 2015, **3**, 3989–3998.
- 35 (a) C. Cheng, R. Fan, Z. Wang, Q. Shao, X. Guo, P. Xie, Y. Yin, Y. Zhang, L. An, Y. Lei, J. E. Ryu, A. Shankar and Z. Guo, *Carbon*, 2017, **125**, 103–112; (b) Z. Wang, R. Wei, J. Gu, H. Liu, C. Liu, C. Luo, J. Kong, Q. Shao, N. Wang, Z. Guo and X. Liu, *Carbon*, 2018, **139**, 1126–1135; (c) C. Wang, V. Murugadoss, J. Kong, Z. He, X. Mai, Q. Shao, Y. Chen, L. Guo, C. Liu, S. Angaiah and Z. Guo, *Carbon*, 2018, **140**, 696–733.
- 36 (a) J. Gu, Y. Li, C. Liang, Y. Tang, L. Tang, Y. Zhang, J. Kong, H. Liu and Z. Guo, *J. Mater. Chem. C*, 2018, **6**, 7652–7660; (b) N. Wu, C. Liu, D. Xu, J. Liu, W. Liu, Q. Shao and Z. Guo, *ACS Sustainable Chem. Eng.*, 2018, **6**, 12471–12480; (c) P. Xie, B. He, F. Dang, J. Lin, R. Fan, C. Hou, H. Liu, J. Zhang, Y. Ma and Z. Guo, *J. Mater. Chem. C*, 2018, **6**, 8812–8822; (d) Y. Song, L. He and X. Zhang, *et al.*, *J. Phys. Chem. C*, 2017, **121**, 24774–24785; (e) C. Luo, W. Duan, X. Yin and J. Kong, *J. Phys. Chem. C*, 2016, **120**, 18721–18732.
- 37 (a) J. Guo, H. Song, H. Liu, C. Luo, Y. Ren, T. Ding, M. A. Khan, D. P. Young, X. Liu, X. Zhang, J. Kong and Z. Guo, *J. Mater. Chem. C*, 2017, **5**, 5334–5344; (b) J. Li, H. Liu, J. Guo, Z. Hu, Z. Wang, B. Wang, L. Liu, Y. Huang and Z. Guo, *J. Mater. Chem. C*, 2017, **5**, 1095–1105.
- 38 (a) K. Zhang, G.-H. Li, L.-M. Feng, N. Wang, J. Guo, K. Sun, K.-X. Yu, J.-B. Zeng, T. Li, Z. Guo and M. Wang, *J. Mater. Chem. C*, 2017, **5**, 9359–9369; (b) P. Xie, H. Li, B. He, F. Dang, J. Lin, R. Fan, C. Hou, H. Liu, J. Zhang, Y. Ma and Z. Guo, *J. Mater. Chem. C*, 2018, **6**, 8812–8822; (c) B. Zhao, J. Deng, R. Zhang, L. Liang, B. Fan, Z. Bai, G. Shao and C. Park, *Eng. Sci.*, 2018, **3**, 5–40; (d) L. Lv, J. Liu, H. Liu, C. Liu, Y. Lu, K. Sun, R. Fan, N. Wang, N. Lu, Z. Guo and E. Wujcik, *Eng. Sci.*, 2018, **2**, 26–42.
- 39 (a) L. Yang, X. Wang, X. Mai, T. Wang, C. Wang, X. Li, V. Murugadoss, Q. Shao, S. Angaiah and Z. Guo, *J. Colloid Interface Sci.*, 2019, **534**, 459–468; (b) Z. Hu, Q. Shao, Y. Huang, L. Yu, D. Zhang, X. Xu, J. Lin, H. Liu and Z. Guo, *Nanotechnology*, 2018, **29**, 185602.
- 40 (a) Y. Li, T. Jing, G. Xu, J. Tian, M. Dong, Q. Shao, B. Wang, Z. Wang, Y. Zheng, C. Yang and Z. Guo, *Polymer*, 2018, **149**, 13–22; (b) Z. Yang, X. Hao, S. Chen, Z. Ma, W. Wang, C. Wang, L. Yue, H. Sun, Q. Shao, V. Murugadoss and Z. Guo, *J. Colloid Interface Sci.*, 2019, **533**, 13–23; (c) P. Zhang, T. Ge, H. Yang, S. Lin, Y. Cao, C. Zhao, H. Liu, A. Umar and Z. Guo, *Sci. Adv. Mater.*, 2018, **10**, 1216–1223; (d) J. Lin, X. Chen, C. Chen, J. Hu, C. Zhou, X. Cai, W. Wang, C. Zheng, R. Zhang, J. Cheng, Z. Guo and H. Liu, *ACS Appl. Mater. Interfaces*, 2018, **10**, 6124–6136.
- 41 Y. Ma, C. Hou, H. Zhang, M. Qiao, Y. Chen, H. Zhang, Q. Zhang and Z. Guo, *J. Mater. Chem. A*, 2017, **5**, 14041–14052.
- 42 H. Yi, H. Wang, Y. Jing, T. Peng, Y. Wang, J. Guo, Q. He, Z. Guo and X. Wang, *J. Mater. Chem. A*, 2015, **3**, 19545–19555.
- 43 H. Wang, Z. Xu, H. Yi, H. Wei, Z. Guo and X. Wang, *Nano Energy*, 2014, **7**, 86–96.
- 44 Q. Luo, H. Ma, Q. Hou, Y. Li, J. Ren, X. Dai, Z. Yao, Y. Zhou, L. Xiang, H. Du, H. He, N. Wang, K. Jiang, H. Lin, H. Zhang and Z. Guo, *Adv. Funct. Mater.*, 2018, **28**, 1706777.
- 45 Y. Guo, Y. Li, X. Lou, J. Guan, Y. Li, X. Mai, H. Liu, C. X. Zhao, N. Wang, C. Yan, G. Gao, H. Yuan, J. Dai, R. Su and Z. Guo, *J. Mater. Sci.*, 2018, **53**, 13790–13800.
- 46 W. Chen, L. Zhang, C. Liu, X. Feng, J. Zhang, L. Guan, L. Mi and S. Cui, *ACS Appl. Mater. Interfaces*, 2018, **10**, 23883–23890.
- 47 J. Huang, Y. Cao, Q. Shao, X. Peng and Z. Guo, *Ind. Eng. Chem. Res.*, 2017, **56**, 10689–10701.

- 48 Y. Wang, B. Wang, J. Wang, Y. Ren, C. Xuan, C. Liu and C. Shen, *J. Hazard. Mater.*, 2018, **344**, 849–856.
- 49 B. Wang, W. Chen, L. Zhang, Z. Li, C. Liu, J. Chen and C. Shen, *Mater. Lett.*, 2017, **188**, 201–204.
- 50 K. Gong, Q. Hu, Y. Xiao, X. Cheng, H. Liu, N. Wang, B. Qiu and Z. Guo, *J. Mater. Chem. A*, 2018, **6**, 11119–11128.
- 51 J. Huang, Y. Li, Y. Cao, F. Peng, Y. Cao, Q. Shao, H. Liu and Z. Guo, *J. Mater. Chem. A*, 2018, **6**, 13062–13074.
- 52 (a) Y. Zhang, M. Zhao, J. Zhang, Q. Shao, J. Li, H. Li, B. Lin, M. Yu, S. Chen and Z. Guo, *J. Polym. Res.*, 2018, **25**, 130; (b) X. Cui, G. Zhu, Y. Pan, Q. Shao, C. Zhao, M. Dong, Y. Zhang and Z. Guo, *Polymer*, 2018, **138**, 203–210; (c) H. Kang, Z. Cheng, H. Lai, H. Ma, Y. Liu, X. Mai, Y. Wang, Q. Shao, L. Xiang, X. Guo and Z. Guo, *Sep. Purif. Technol.*, 2018, **201**, 193–204; (d) X. Guo, S. Ge, J. Wang and X. Zhang, *et al.*, *Polymer*, 2018, **143**, 155–163; (e) J. Li, S. Ge, J. Wang, H. Du, K. Song, Z. Fei, Q. Shao and Z. Guo, *Colloids Surf., A*, 2017, **537**, 334–342.
- 53 (a) H. Gu, H. Zhang, J. Lin, Q. Shao, D. P. Young, L. Sun, T. D. Shen and Z. Guo, *Polymer*, 2018, **143**, 324–330; (b) H. Gu, J. Guo, H. Wei, X. Zhang, J. Zhu, L. Shao, Y. Huang, N. Haldolaarachchige, D. P. Young, S. Wei and Z. Guo, *Polymer*, 2014, **55**, 944–950; (c) H. Gu, J. Guo, M. A. Khan, D. P. Young, T. D. Shen, S. Wei and Z. Guo, *Phys. Chem. Chem. Phys.*, 2016, **18**, 19536–19543.
- 54 (a) H. Gu, J. Guo, H. Wei, S. Guo, J. Liu, Y. Huang, M. A. Khan, X. Wang, D. P. Young, S. Wei and Z. Guo, *Adv. Mater.*, 2015, **27**, 6277–6282; (b) H. Gu, J. Guo, Q. He, Y. Jiang, Y. Huang, N. Haldolaarachchige, Z. Luo, D. P. Young, S. Wei and Z. Guo, *Nanoscale*, 2014, **6**, 181–189.
- 55 Z. Hu, D. Zhang, F. Lu, W. Yuan, X. Xu, Q. Zhang, H. Liu, Q. Shao, Z. Guo and Y. Huang, *Macromolecules*, 2018, **51**, 5294–5303.
- 56 (a) Y. Li, Y. Zheng, P. Zhan, G. Zheng, K. Dai, C. Liu and C. Shen, *Sens. Actuators, B*, 2018, **255**, 2809–2819; (b) Y. Lu, M. C. Biswas, Z. Guo, J. W. Jeon and E. K. Wujcik, *Biosens. Bioelectron.*, 2019, **123**, 167–177.
- 57 X. Cao, X. Wei, G. Li, C. Hu, K. Dai, J. Guo, G. Zheng, C. Liu, C. Shen and Z. Guo, *Polymer*, 2017, **112**, 1–9.
- 58 G. Li, C. Hu, W. Zhai, S. Zhao, G. Zheng, K. Dai, C. Liu and C. Shen, *Mater. Lett.*, 2016, **182**, 314–317.
- 59 H. Liu, W. Huang, X. Yang, K. Dai, G. Zheng, C. Liu, C. Shen, X. Yan, J. Guo and Z. Guo, *J. Mater. Chem. C*, 2016, **4**, 4459–4469.
- 60 Z. Xu, N. Wang, N. Li, G. Zheng, K. Dai, C. Liu and C. Shen, *Composites, Part B*, 2016, **94**, 45–51.
- 61 X. Cao, Y. Lan, Y. Wei, G. Zheng, K. Dai, C. Liu and C. Shen, *Mater. Lett.*, 2015, **159**, 276–279.
- 62 H. Deng and Q. Fu, *Macromol. Rapid Commun.*, 2017, **38**.
- 63 J. Lee, M. Lim, J. Yoon, M. S. Kim, B. Choi, D. M. Kim, D. H. Kim, I. Park and S. J. Choi, *ACS Appl. Mater. Interfaces*, 2017, **9**, 26279–26285.
- 64 L. Xie and Y. Zhu, *Polym. Compos.*, 2018, **39**, 2985–2996.
- 65 H. Liu, M. Dong, W. Huang, J. Gao, K. Dai, J. Guo, G. Zheng, C. Liu, C. Shen and Z. Guo, *J. Mater. Chem. C*, 2017, **5**, 73–83.
- 66 H. Liu, J. Gao, W. Huang, K. Dai, G. Zheng, C. Liu, C. Shen, X. Yan, J. Guo and Z. Guo, *Nanoscale*, 2016, **8**, 12977–12989.
- 67 H. Liu, W. Huang, J. Gao, K. Dai, G. Zheng, C. Liu, C. Shen, X. Yan, J. Guo and Z. Guo, *Appl. Phys. Lett.*, 2016, **2018**, 011904.
- 68 H. Liu, Y. Li, K. Dai, G. Zheng, C. Liu, C. Shen, X. Yan, J. Guo and Z. Guo, *J. Mater. Chem. C*, 2016, **4**, 157–166.
- 69 H. Liu, W. Huang, J. Gao, K. Dai, G. Zheng, C. Liu, C. Shen, X. Yan, J. Guo and Z. Guo, *Appl. Phys. Lett.*, 2016, **108**, 011904.
- 70 S. Ding, J. Jiu, Y. Gao, Y. Tian, T. Araki, T. Sugahara, S. Nagao, M. Nogi, H. Koga, K. Suganuma and H. Uchida, *ACS Appl. Mater. Interfaces*, 2016, **8**, 6190–6199.
- 71 Y. Ding, J. Zhu, C. Wang, B. Dai, Y. Li, Y. Qin, F. Xu, Q. Peng, Z. Yang, J. Bai, W. Cao, Y. Yuan and Y. Li, *Carbon*, 2016, **104**, 133–140.
- 72 X. Dong, Y. Wei, S. Chen, Y. Lin, L. Liu and J. Li, *Compos. Sci. Technol.*, 2018, **155**, 108–116.
- 73 S. Seyedin, J. M. Razal, P. C. Innis, A. Jeiranikhameneh, S. Beirne and G. G. Wallace, *ACS Appl. Mater. Interfaces*, 2015, **7**, 21150–21158.
- 74 Z. Tang, S. Jia, F. Wang, C. Bian, Y. Chen, Y. Wang and B. Li, *ACS Appl. Mater. Interfaces*, 2018, **10**, 6624–6635.
- 75 L. Lin, H. Deng, X. Gao, S. Zhang, E. Bilotti, T. Peijs and Q. Fu, *Polym. Int.*, 2013, **62**, 134–140.
- 76 G. W. Huang, H. M. Xiao and S. Y. Fu, *Sci. Rep.*, 2015, **5**, 13971.
- 77 Y. Li, B. Zhou, G. Zheng, X. Liu, T. Li, C. Yan, C. Cheng, K. Dai, C. Liu, C. Shen and Z. Guo, *J. Mater. Chem. C*, 2018, **6**, 2258–2269.
- 78 X. Guan, G. Zheng, K. Dai, C. Liu, X. Yan, C. Shen and Z. Guo, *ACS Appl. Mater. Interfaces*, 2016, **8**, 14150–14159.
- 79 S. Yao and Y. Zhu, *Nanoscale*, 2014, **6**, 2345–2352.
- 80 S. Gong, W. Schwalb, Y. Wang, Y. Chen, Y. Tang, J. Si, B. Shirinzadeh and W. Cheng, *Nat. Commun.*, 2014, **5**, 3132.
- 81 Y. Q. Li, W. B. Zhu, X. G. Yu, P. Huang, S. Y. Fu, N. Hu and K. Liao, *ACS Appl. Mater. Interfaces*, 2016, **8**, 33189–33196.
- 82 G. Ambrosetti, C. Grimaldi, I. Balberg, T. Maeder, A. Danani and P. Ryser, *Phys. Rev. B: Condens. Matter Mater. Phys.*, 2010, **81**, 155434.
- 83 J. Gurland, *Trans. Metall. Soc. AIME*, 1966, **212**, 642–646.
- 84 A. Goldel, G. Kasaliwal and P. Potschke, *Macromol. Rapid Commun.*, 2009, **30**, 423–429.
- 85 B. P. Grady, *Macromol. Rapid Commun.*, 2010, **31**, 247–257.
- 86 Y.-H. Ji, Y. Liu, Y.-Q. Li, H.-M. Xiao, S.-S. Du, J.-Y. Zhang, N. Hu and S.-Y. Fu, *Compos. Sci. Technol.*, 2016, **132**, 57–67.
- 87 X. Cheng, T. Yokozeki, L. Wu, H. Wang, J. Zhang, J. Koyanagi, Z. Weng and Q. Sun, *Composites, Part A*, 2016, **90**, 243–249.
- 88 C. Lee, L. Jug and E. Meng, *Appl. Phys. Lett.*, 2013, **102**, 183511.
- 89 K. Liu, S. Chen, Y. Luo and L. Liu, *RSC Adv.*, 2014, **4**, 41876–41885.
- 90 E. Bilotti, H. Zhang, H. Deng, R. Zhang, Q. Fu and T. Peijs, *Compos. Sci. Technol.*, 2013, **74**, 85–90.

- 91 J. Y. Oh, G. H. Jun, S. Jin, H. J. Ryu and S. H. Hong, *ACS Appl. Mater. Interfaces*, 2016, **8**, 3319–3325.
- 92 S. Zhao, H. Zhao, G. Li, K. Dai, G. Zheng, C. Liu and C. Shen, *Mater. Lett.*, 2014, **129**, 72–75.
- 93 W. Zhai, S. Zhao, Y. Wang, G. Zheng, K. Dai, C. Liu and C. Shen, *Composites, Part A*, 2018, **105**, 68–77.
- 94 S. Zhao, G. Li, H. Liu, K. Dai, G. Zheng, X. Yan, C. Liu, J. Chen, C. Shen and Z. Guo, *Adv. Mater. Interfaces*, 2017, **4**, 1700265.
- 95 Y. Wei, Z. Li, X. Liu, K. Dai, G. Zheng, C. Liu, J. Chen and C. Shen, *Colloid Polym. Sci.*, 2014, **292**, 2891–2898.
- 96 K. Dai, S. Zhao, W. Zhai, G. Zheng, C. Liu, J. Chen and C. Shen, *Composites, Part A*, 2013, **55**, 11–18.
- 97 S. Zhao, D. Lou, P. Zhan, G. Li, K. Dai, J. Guo, G. Zheng, C. Liu, C. Shen and Z. Guo, *J. Mater. Chem. C*, 2017, **5**, 8233–8242.
- 98 T. Gong, M.-Q. Liu, H. Liu, S.-P. Peng, T. Li, R.-Y. Bao, W. Yang, B.-H. Xie, M.-B. Yang and Z. Guo, *Polymer*, 2017, **110**, 1–11.
- 99 Y. Bao, L. Xu, H. Pang, D.-X. Yan, C. Chen, W.-Q. Zhang, J.-H. Tang and Z.-M. Li, *J. Mater. Sci.*, 2013, **48**, 4892–4898.
- 100 Y. Lan, H. Liu, X. Cao, S. Zhao, K. Dai, X. Yan, G. Zheng, C. Liu, C. Shen and Z. Guo, *Polymer*, 2016, **97**, 11–19.
- 101 M. A. Poothanari, J. Abraham, N. Kalarikkal and S. Thomas, *Ind. Eng. Chem. Res.*, 2018, **57**, 4287–4297.
- 102 H. Bizhani, V. Nayyeri, A. Katbab, A. Jalali-Arani and H. Nazockdast, *Eur. Polym. J.*, 2018, **100**, 209–218.
- 103 W. Huang, K. Dai, Y. Zhai, H. Liu, P. Zhan, J. Gao, G. Zheng, C. Liu and C. Shen, *ACS Appl. Mater. Interfaces*, 2017, **9**, 42266–42277.
- 104 M. Z. Seyedin, J. M. Razal, P. C. Innis and G. G. Wallace, *Adv. Funct. Mater.*, 2014, **24**, 2957–2966.
- 105 Q. Fan, Z. Qin, S. Gao, Y. Wu, J. Pionteck, E. Mäder and M. Zhu, *Carbon*, 2012, **50**, 4085–4092.
- 106 S. Chen, Y. Wei, S. Wei, Y. Lin and L. Liu, *J. Mater. Chem. C*, 2016, **8**, 25563–25570.
- 107 X. Wang, J. Sparkman and J. Gou, *Compos. Commun.*, 2017, **3**, 1–6.
- 108 G. Li, K. Dai, M. Ren, Y. Wang, G. Zheng, C. Liu and C. Shen, *J. Mater. Chem. C*, 2018, **6**, 6575–6583.
- 109 S. Zhao, J. Li, D. Cao, Y. Gao, W. Huang, G. Zhang, R. Sun and C.-P. Wong, *J. Mater. Chem. C*, 2016, **4**, 6666–6674.
- 110 S. Wang, X. Zhang, X. Wu and C. Lu, *Soft Matter*, 2016, **12**, 845–852.
- 111 X. Wu, C. Lu, Y. Han, Z. Zhou, G. Yuan and X. Zhang, *Compos. Sci. Technol.*, 2016, **124**, 44–51.
- 112 Y. Lin, X. Dong, S. Liu, S. Chen, Y. Wei and L. Liu, *ACS Appl. Mater. Interfaces*, 2016, **8**, 24143–24151.
- 113 J. Cao, X. Zhang, X. Wu, S. Wang and C. Lu, *Carbohydr. Polym.*, 2016, **140**, 88–95.
- 114 Z.-M. Dang, M.-J. Jiang, D. Xie, S.-H. Yao, L.-Q. Zhang and J. Bai, *J. Appl. Phys.*, 2008, **104**, 024114.
- 115 Y. Wang, Y. Jia, Y. Zhou, Y. Wang, G. Zheng, K. Dai, C. Liu and C. Shen, *J. Mater. Chem. C*, 2018, **6**, 8160–8170.
- 116 U.-H. Shin, D.-W. Jeong, S.-M. Park, S.-H. Kim, H. W. Lee and J.-M. Kim, *Carbon*, 2014, **80**, 396–404.
- 117 C. Wang, X. Li, E. Gao, M. Jian, K. Xia, Q. Wang, Z. Xu, T. Ren and Y. Zhang, *Adv. Mater.*, 2016, **28**, 6640–6648.
- 118 M. Amjadi, M. Turan, C. P. Clementson and M. Sitti, *ACS Appl. Mater. Interfaces*, 2016, **8**, 5618–5626.
- 119 R. Xu, Y. Lu, C. Jiang, J. Chen, P. Mao, G. Gao, L. Zhang and S. Wu, *ACS Appl. Mater. Interfaces*, 2014, **6**, 13455–13460.
- 120 J.-H. Kong, N.-S. Jang, S.-H. Kim and J.-M. Kim, *Carbon*, 2014, **77**, 199–207.
- 121 H. Niu, H. Zhou, H. Wang and T. Lin, *Macromol. Mater. Eng.*, 2016, **301**, 707–713.
- 122 X. Li, R. Zhang, W. Yu, K. Wang, J. Wei, D. Wu, A. Cao, Z. Li, Y. Cheng, Q. Zheng, R. S. Ruoff and H. Zhu, *Sci. Rep.*, 2012, **2**, 870.
- 123 X. Zhou, L. Zhu, L. Fan, H. Deng and Q. Fu, *ACS Appl. Mater. Interfaces*, 2018, **10**, 31655–31663.
- 124 X. Liu, J. Kruckel, G. Zheng and D. W. Schubert, *ACS Appl. Mater. Interfaces*, 2013, **5**, 8857–8860.
- 125 M. Qu, F. Nilsson, Y. Qin, G. Yang, Y. Pan, X. Liu, G. Hernandez Rodriguez, J. Chen, C. Zhang and D. W. Schubert, *Compos. Sci. Technol.*, 2017, **150**, 24–31.
- 126 X. Liu, J. Krückel, G. Zheng and D. W. Schubert, *Compos. Sci. Technol.*, 2014, **100**, 99–104.
- 127 X. Liu, Y. Pan, G. Zheng and D. W. Schubert, *Compos. Sci. Technol.*, 2016, **128**, 1–7.
- 128 X. Liu, Y. Pan, X. Hao, K. Dai and D. W. Schubert, *J. Appl. Polym. Sci.*, 2016, 133.
- 129 Z. Zhou, X. Zhang, X. Wu and C. Lu, *Compos. Sci. Technol.*, 2016, **125**, 1–8.
- 130 M. Tian, Y. Wang, L. Qu, S. Zhu, G. Han, X. Zhang, Q. Zhou, M. Du and S. Chi, *Synth. Met.*, 2016, **219**, 11–19.
- 131 J. P. Wang, P. Xue and X. M. Tao, *Mater. Sci. Eng., A*, 2011, **528**, 2863–2869.
- 132 G. Latessa, F. Brunetti, A. Reale, G. Saggio and A. Di Carlo, *Sens. Actuators, B*, 2009, **139**, 304–309.
- 133 H. C. Chu, Y. C. Chang, Y. Lin, S. H. Chang, W. C. Chang, G. A. Li and H. Y. Tuan, *ACS Appl. Mater. Interfaces*, 2016, **8**, 13009–13017.
- 134 Y. Wei, S. Chen, F. Li, Y. Lin, Y. Zhang and L. Liu, *ACS Appl. Mater. Interfaces*, 2015, **7**, 14182–14191.
- 135 K. K. Kim, S. Hong, H. M. Cho, J. Lee, Y. D. Suh, J. Ham and S. H. Ko, *Nano Lett.*, 2015, **15**, 5240–5247.
- 136 P. Lee, J. Lee, H. Lee, J. Yeo, S. Hong, K. H. Nam, D. Lee, S. S. Lee and S. H. Ko, *Adv. Mater.*, 2012, **24**, 3326–3332.
- 137 Y. Hu, T. Zhao, P. Zhu, Y. Zhu, X. Shuai, X. Liang, R. Sun, D. D. Lu and C.-P. Wong, *J. Mater. Chem. C*, 2016, **4**, 5839–5848.
- 138 T. Yang, X. Li, X. Jiang, S. Lin, J. Lao, J. Shi, Z. Zhen, Z. Li and H. Zhu, *Mater. Horiz.*, 2016, **3**, 248–255.
- 139 H. Liu, L.-l. Zhu, Y. He and B.-w. Cheng, *Mater. Des.*, 2017, **113**, 254–263.
- 140 Y. Yang, Z. Li, W. Ji, C. Sun, H. Deng and Q. Fu, *Composites, Part A*, 2018, **104**, 24–31.
- 141 M.-J. Jiang, Z.-M. Dang, H.-P. Xu, S.-H. Yao and J. Bai, *Appl. Phys. Lett.*, 2007, **91**, 072907.
- 142 J. Zhao, K. Dai, X. Xu, G. Zheng, C. Liu and J. Chen, *Polym.-Plast. Technol. Eng.*, 2013, **52**, 1303–1307.

- 143 Y. Qu, K. Dai, J. Zhao, G. Zheng, C. Liu, J. Chen and C. Shen, *Colloid Polym. Sci.*, 2013, **292**, 945–951.
- 144 C. Hu, Z. Li, Y. Wang, J. Gao, K. Dai, G. Zheng, C. Liu, C. Shen, H. Song and Z. Guo, *J. Mater. Chem. C*, 2017, **5**, 2318–2328.
- 145 Y. Zheng, Y. Li, K. Dai, M. Liu, K. Zhou, G. Zheng, C. Liu and C. Shen, *Composites, Part A*, 2017, **101**, 41–49.
- 146 Y. Zheng, Y. Li, Z. Li, Y. Wang, K. Dai, G. Zheng, C. Liu and C. Shen, *Compos. Sci. Technol.*, 2017, **139**, 64–73.
- 147 D. Cho, J. Park, J. Kim, T. Kim, J. Kim, I. Park and S. Jeon, *ACS Appl. Mater. Interfaces*, 2017, **9**, 17369–17378.
- 148 J. Ge, H. B. Yao, X. Wang, Y. D. Ye, J. L. Wang, Z. Y. Wu, J. W. Liu, F. J. Fan, H. L. Gao, C. L. Zhang and S. H. Yu, *Angew. Chem., Int. Ed. Engl.*, 2013, **52**, 1654–1659.
- 149 D. Kang, P. V. Pikhitsa, Y. W. Choi, C. Lee, S. S. Shin, L. Piao, B. Park, K. Y. Suh, T. I. Kim and M. Choi, *Nature*, 2014, **516**, 222–226.
- 150 A. Kim, J. Ahn, H. Hwang, E. Lee and J. Moon, *Nanoscale*, 2017, **9**, 5773–5778.
- 151 N. Wang, Z. Xu, P. Zhan, K. Dai, G. Zheng, C. Liu and C. Shen, *J. Mater. Chem. C*, 2017, **5**, 4408–4418.
- 152 H. Deng, L. Lin, M. Ji, S. Zhang, M. Yang and Q. Fu, *Prog. Polym. Sci.*, 2014, **39**, 627–655.
- 153 H. Pang, L. Xu, D.-X. Yan and Z.-M. Li, *Prog. Polym. Sci.*, 2014, **39**, 1908–1933.
- 154 I. Balberg, *Phys. Rev. Lett.*, 1987, **59**, 1305–1308.
- 155 I. Alig, P. Pötschke, D. Lellinger, T. Skipa, S. Pegel, G. R. Kasaliwal and T. Villmow, *Polymer*, 2012, **53**, 4–28.
- 156 W. Zhai, R. Sun, H. Sun, M. Ren, K. Dai, G. Zheng, C. Liu and C. Shen, *Mater. Lett.*, 2018, **229**, 13–16.
- 157 Y. Lin, S. Liu, J. Peng and L. Liu, *Compos. Sci. Technol.*, 2016, **131**, 40–47.
- 158 A. B. Oskouyi, U. Sundararaj and P. Mertiny, *Materials*, 2014, **7**, 2501–2521.
- 159 W. Luo, T. Wu, B. Chen, M. Liang and H. Zou, *ACS Appl. Mater. Interfaces*, 2017, **9**, 43239–43249.
- 160 H. Yazdani, K. Hatami, E. Khosravi, K. Harper and B. P. Grady, *Carbon*, 2014, **79**, 393–405.
- 161 S. Zheng, J. Deng, L. Yang, D. Ren, S. Huang, W. Yang, Z. Liu and M. Yang, *Compos. Sci. Technol.*, 2014, **97**, 34–40.
- 162 W. Yi, Y. Wang, G. Wang and X. Tao, *Polym. Test.*, 2012, **31**, 677–684.
- 163 J. Zhao, K. Dai, C. Liu, G. Zheng, B. Wang, C. Liu, J. Chen and C. Shen, *Composites, Part A*, 2013, **48**, 129–136.
- 164 H. Xu, Z. Zeng, Z. Wu, L. Zhou, Z. Su, Y. Liao and M. Liu, *Compos. Sci. Technol.*, 2017, **149**, 246–253.
- 165 Z. Zeng, M. Liu, H. Xu, Y. Liao, F. Duan, L.-m. Zhou, H. Jin, Z. Zhang and Z. Su, *Carbon*, 2017, **121**, 490–501.
- 166 A. A. El-Gamal, H. M. Alsubaiqi and H. H. Hassan, *J. Macromol. Sci., Part B: Phys.*, 2017, **56**, 697–708.
- 167 L. Flandin, A. Chang, S. Nazarenko, A. Hiltner and E. Baer, *J. Appl. Polym. Sci.*, 2000, **77**, 894–905.
- 168 K. Yamaguchi, J. J. C. Busfield and A. G. Thomas, *J. Polym. Sci., Part B: Polym. Phys.*, 2003, **41**, 2079–2089.
- 169 V. Jha, A. G. Thomas, M. Bennett and J. J. C. Busfield, *J. Appl. Polym. Sci.*, 2010, **116**, 541–546.
- 170 R. Zhang, H. Deng, R. Valenca, J. Jin, Q. Fu, E. Bilotti and T. Peijs, *Compos. Sci. Technol.*, 2013, **74**, 1–5.
- 171 F. Mai, Y. Habibi, J.-M. Raquez, P. Dubois, J.-F. Feller, T. Peijs and E. Bilotti, *Polymer*, 2013, **54**, 6818–6823.
- 172 R. Zhang, H. Deng, R. Valenca, J. Jin, Q. Fu, E. Bilotti and T. Peijs, *Sens. Actuators, A*, 2012, **179**, 83–91.
- 173 R. Zhang, M. Baxendale and T. Peijs, *Phys. Rev. B: Condens. Matter Mater. Phys.*, 2007, **76**.
- 174 X. Wang, X. Liu, H. Yuan, H. Liu, C. Liu, T. Li, C. Yan, X. Yan, C. Shen and Z. Guo, *Mater. Des.*, 2018, **139**, 372–379.
- 175 K.-H. Liao, Y. T. Park, A. Abdala and C. Macosko, *Polymer*, 2013, **54**, 4555–4559.
- 176 S. Liu, Y. Lin, Y. Wei, S. Chen, J. Zhu and L. Liu, *Compos. Sci. Technol.*, 2017, **146**, 110–118.
- 177 L. Lu, X. Wei, Y. Zhang, G. Zheng, K. Dai, C. Liu and C. Shen, *J. Mater. Chem. C*, 2017, **5**, 7035–7042.
- 178 X. Wu, C. Lu, X. Zhang and Z. Zhou, *J. Mater. Chem. A*, 2015, **3**, 13317–13323.
- 179 Y. Wei, S. Chen, X. Dong, Y. Lin and L. Liu, *Carbon*, 2017, **113**, 395–403.
- 180 Y. Zhou, Y. Zhou, H. Deng and Q. Fu, *Composites, Part A*, 2017, **96**, 99–109.
- 181 L. Lin, S. Liu, Q. Zhang, X. Li, M. Ji, H. Deng and Q. Fu, *ACS Appl. Mater. Interfaces*, 2013, **5**, 5815–5824.
- 182 K. Ke, P. Pötschke, N. Wiegand, B. Krause and B. Voit, *ACS Appl. Mater. Interfaces*, 2016, **8**, 14190–14199.
- 183 H. Zhao and J. Bai, *ACS Appl. Mater. Interfaces*, 2015, **7**, 9652–9659.
- 184 S. Zhao, D. Lou, G. Li, Y. Zheng, G. Zheng, K. Dai, C. Liu, Y. Jiang and C. Shen, *Compos. Sci. Technol.*, 2018, **163**, 18–25.
- 185 H. Zhou, H. Deng, L. Zhang, Z. Wu, S. Deng, W. Yang, Q. Zhang, F. Chen and Q. Fu, *Composites, Part A*, 2016, **82**, 20–33.
- 186 A. Malliaris and D. T. Turner, *J. Appl. Phys.*, 1971, **42**, 614–618.
- 187 M. Wang, K. Zhang, X. X. Dai, Y. Li, J. Guo, H. Liu, G. H. Li, Y. J. Tan, J. B. Zeng and Z. Guo, *Nanoscale*, 2017, **9**, 11017–11026.
- 188 X. Wei, X. Cao, Y. Wang, G. Zheng, K. Dai, C. Liu and C. Shen, *Compos. Sci. Technol.*, 2017, **149**, 166–177.
- 189 S. Wu, J. Zhang, R. B. Ladani, A. R. Ravindran, A. P. Mouritz, A. J. Kinloch and C. H. Wang, *ACS Appl. Mater. Interfaces*, 2017, **9**, 14207–14215.
- 190 Q. Li, J. Li, D. Tran, C. Luo, Y. Gao, C. Yu and F. Xuan, *J. Mater. Chem. C*, 2017, **5**, 11092–11099.
- 191 Y. H. Wu, H. Z. Liu, S. Chen, X. C. Dong, P. P. Wang, S. Q. Liu, Y. Lin, Y. Wei and L. Liu, *ACS Appl. Mater. Interfaces*, 2017, **9**, 20098–20105.
- 192 Z. Ma, A. Wei, J. Ma, L. Shao, H. Jiang, D. Dong, Z. Ji, Q. Wang and S. Kang, *Nanoscale*, 2018, **10**, 7116–7126.
- 193 X. Wu, Y. Han, X. Zhang, Z. Zhou and C. Lu, *Adv. Funct. Mater.*, 2016, **26**, 6246–6256.
- 194 L. Li, C. Zhu, Y. Wu, J. Wang, T. Zhang and Y. Liu, *RSC Adv.*, 2015, **5**, 62905–62912.

- 195 Y. Tang, S. Gong, Y. Chen, L. W. Yap and W. Cheng, *ACS Nano*, 2014, **8**, 5707–5714.
- 196 J. Zou, J. Liu, A. S. Karakoti, A. Kumar, D. Joung, Q. Li, S. I. Khondaker, S. Seal and L. Zhai, *ACS Nano*, 2010, **4**, 7293–7302.
- 197 Y. Tang, K. L. Yeo, Y. Chen, L. W. Yap, W. Xiong and W. Cheng, *J. Mater. Chem. A*, 2013, **1**, 6723.
- 198 H. Hu, Z. Zhao, W. Wan, Y. Gogotsi and J. Qiu, *ACS Appl. Mater. Interfaces*, 2014, **6**, 3242–3249.
- 199 H. Vandeparre, Q. Liu, I. R. Mineev, Z. Suo and S. P. Lacour, *Adv. Mater.*, 2013, **25**, 3117–3121.
- 200 A. Chortos, J. Lim, J. W. To, M. Vosgueritchian, T. J. Dusseault, T. H. Kim, S. Hwang and Z. Bao, *Adv. Mater.*, 2014, **26**, 4253–4259.
- 201 P. Slobodian, P. Riha and P. Saha, *Carbon*, 2012, **50**, 3446–3453.
- 202 X. Liao, Z. Zhang, Q. Liao, Q. Liang, Y. Ou, M. Xu, M. Li, G. Zhang and Y. Zhang, *Nanoscale*, 2016, **8**, 13025–13032.
- 203 H. L. Filiatrault, R. S. Carmichael, R. A. Boutette and T. B. Carmichael, *ACS Appl. Mater. Interfaces*, 2015, **7**, 20745–20752.
- 204 M. Santhiago, C. C. Correa, J. S. Bernardes, M. P. Pereira, L. J. M. Oliveira, M. Strauss and C. C. B. Bufon, *ACS Appl. Mater. Interfaces*, 2017, **9**, 24365–24372.
- 205 F. Han, J. Li, S. Zhao, Y. Zhang, W. Huang, G. Z. Zhang, R. Sun and C.-P. W. Wong, *J. Mater. Chem. C*, 2017, **5**, 10167–10175.
- 206 C. Wang, J. Zhao, C. Ma, J. Sun, L. Tian, X. Li, F. Li, X. Han, C. Liu, C. Shen, L. Dong, J. Yang and C. Pan, *Nano Energy*, 2017, **34**, 578–585.
- 207 H. Liu, H. Jiang, F. Du, D. Zhang, Z. Li and H. Zhou, *ACS Sustainable Chem. Eng.*, 2017, **5**, 10538–10543.
- 208 T. Wang, Y. Zhang, Q. Liu, W. Cheng, X. Wang, L. Pan, B. Xu and H. Xu, *Adv. Funct. Mater.*, 2018, **28**, 1705551.
- 209 L. Li, Y. Bai, L. Li, S. Wang and T. Zhang, *Adv. Mater.*, 2017, **29**, 1702517.
- 210 X. Su, H. Li, X. Lai, Z. Chen and X. Zeng, *ACS Appl. Mater. Interfaces*, 2018, **10**, 10587–10597.
- 211 L. Cai, J. Li, P. Luan, H. Dong, D. Zhao, Q. Zhang, X. Zhang, M. Tu, Q. Zeng, W. Zhou and S. Xie, *Adv. Funct. Mater.*, 2012, **22**, 5238–5244.
- 212 S.-H. Bae, Y. Lee, B. K. Sharma, H.-J. Lee, J.-H. Kim and J.-H. Ahn, *Carbon*, 2013, **51**, 236–242.
- 213 M. Li, H. Li, W. Zhong, Q. Zhao and D. Wang, *ACS Appl. Mater. Interfaces*, 2014, **6**, 1313–1319.
- 214 B. Zhang, J. Lei, D. Qi, Z. Liu, Y. Wang, G. Xiao, J. Wu, W. Zhang, F. Huo and X. Chen, *Adv. Funct. Mater.*, 2018, **28**, 1801683.
- 215 Y. Qin, Q. Peng, Y. Ding, Z. Lin, C. Wang, Y. Li, F. Xu, J. Li, Y. Yuan, X. He and Y. Li, *ACS Nano*, 2015, **9**, 8933–8941.